Università degli Studi di Padova

Dipartimento dei Beni Culturali: Archeologia,
Storia dell'Arte, del Cinema e della Musica

Master Degree in
ARCHAEOLOGICAL SCIENCES

Curriculum in
APPLIED SCIENCES TO CULTURAL HERITAGE MATERIALS AND SITES

Mechanical characteristics of Roman concrete & their relationship with materials' composition:

The case studies of Roman theatre of Aquileia & Diocletian Baths in Rome

Supervisor:

Prof. Michele Secco

Co-supervisor:

Prof. Simone Dilaria

Prof. Enrico Garbin

Dr. Valeria Razzante

Master Candidate

Bareea Tariq

2078588

ACADEMIC YEAR 2022/2023

Table of Contents

List of figures iii

List of tables vi

Acknowledgements vii

Ringraziamenti viii

Abstract ix

Sommario x

1. Introduction 1

1.1. Research Objectives 2

2. Opus Caementicium 3

3. Historical context of the sites 5

3.1. Roman Theater of Aquileia 5

3.2. Diocletian Baths, Rome 8

4. Sites & Samples 11

4.1. Roman Theater of Aquileia 11

4.2. Diocletian Baths, Rome 16

5. Materials & Methods 19

5.1. Optical Microscopy 19

5.2. XRPD 21

5.3. SEM-EDS 22

5.4. Mechanical Tests 24

6. Results 26

6.1. Optical Microscopy 26

6.1.1. Aquileia 27

6.1.2. Diocletian Baths 33

6.2. SEM-EDS 35

6.2.1. Group 1: CM_69 35

6.2.2. Group 2: CM_89 39
6.2.3. Group 3: CM_66 41
6.2.4. Outlier: CM_76 43
6.2.5. Diocletian baths: DB_V1 44
6.3. XRPD 47
6.3.1. Aquileia 47
6.3.2. Diocletian Baths: 49
6.4. Mechanical Testing 50
7. Discussion and Conclusions 55
8. Bibliography 57

List of figures

Figure 1 Ancient Roman city of Aquileia 5
Figure 2 The Roman theatre in Aquileia. (a) Reconstructive plan of the building with indication of the excavated sectors (in dark grey); (b) Reconstructive cross section of the theatre, from the ima cavea to the scaenae frons wall, with stratigraphic sketches of the floor preparations of the orchestra and hyposcaenium. (Source: Dilaria et al. 2023) 7
Figure 3 Baths of Diocletian, with the basilica of Santa Maria degli Angeli e dei Martiri built in the remains of the baths 8
Figure 4 The location of the baths in Rome during Antiquity 8
Figure 5 Reconstructed floorplan:(1) Caldarium, (2) Tepidarium, (3) Frigidarium, (4) Natatio, (5) Palaestra, (6) main entrance, (7) Exedra 9
Figure 6 The church facade: an apse in the wall of the caldarium of the Baths of Diocletian 10
Figure 7 Sampling activities at the Roman theater of Aquileia 11
Figure 8 Location of the site and sampling points from the geognostic survey campaigns of June 2021 (Source: Geoalpina S.r..l.) 12
Figure 9 Core drills from the foundational layer with sampling points and their relative heights 15
Figure 10 Sampling process at the Basilica of Santa Maria degli Angeli (Source: SO.IN.G. strutture e ambiente S.r.l.) 16
Figure 11 Location of the cores inside the Baths of Diocletian, Rome (Source: SO.IN.G. strutture e ambiente S.r.l.) 17
Figure 12 Philips X'Pert PRO diffractometer, Bragg-Brentano geometry with Bragg-Brentano HD optics, cobalt source, X'Celerator detector, and Anton Paar HTK16 hot stage. (source: https://www.geoscienze.unipd.it/diffrattometria-x-polveri) 22
Figure 13 COXEM EM-30AX Tabletop SEM with STEM detector at Insertion position using the side accessory port 23
Figure 14 Micrographs of Group 1 samples showing general composition: CM_69, CM_88 and CM_91 under plain polarized light (a, c & e) and cross polarized light (b, d & f) 1.6x magnification (Scale bar: 1mm) 27
Figure 15 Sample CM_69 showing micrographs of dolomitic aggregate exhibiting clear reaction edges in (a) plain olarized light and (b) cross polarized light 1.6x magnification (Scale bar: 1mm) 28

Figure 16 Micrographs of Group 2 samples showing general composition: CM_70, CM_85 and CM_89 under plain polarized light (a, c & e) and cross polarized light (b, d & f) 1.6x magnification (Scale bar: 1mm).....29
Figure 17 Sample CM_89 showing micrographs of dolomitic aggregates and brick fragments exhibiting clear reaction edges in (a) plain polarized light and (b) cross polarized light 1.6x magnification (Scale bar: 1mm).....30
Figure 18 Micrographs of Group 3 samples showing general composition: CM_65 and CM_66 under plain polarized light (a & c) and cross polarized light (b & d) 1.6x magnification (Scale bar: 1mm).....31
Figure 19 Micrographs of CM_76 showing general composition under plain polarized light (a) and cross polarized light (b) 1.6x magnification (Scale bar: 1mm) 31
Figure 20 Micrographs of Diocletian baths samples showing general composition: DB_C1, DB_C2, DB_C3, DB_C4, DB_V1 & DB_V2 under plain polarized light (a, c, e, i & k) and cross polarized light (b, d, f, j & l) 1.6x magnification (Scale bar: 1mm).....34
Figure 21 SEM-BSE micrographs of the sample showing a lump at 100x magnification (left) and focused on the lump at 2.0kx highlighting selected areas of EDS analysis (right).....35
Figure 22 EDS microanalysis of sample CM_69 with areas highlighted in Figure 21 36
Figure 23 SEM-BSE micrographs of the sample showing a chert aggregate with reaction edges at 100x magnification (left) and focused on the reaction edge at 500x highlighting selected areas of EDS analysis (right) 37
Figure 24 EDS microanalysis of sample CM_69 with areas highlighted in Figure 23 38
Figure 25 SEM-BSE micrographs of the sample showing a chert aggregates at 100x magnification (left) and highlighting selected areas of EDS analysis (right).....38
Figure 26 EDS microanalysis of sample CM_69 with areas highlighted in Figure 25 38
Figure 27 SEM-BSE micrographs of the sample showing a lump at 100x magnification (left) and focused on the lump at 2.0kx highlighting selected areas of EDS analysis (right).....39
Figure 28 EDS microanalysis of sample CM_89 with areas highlighted in Figure 27 39
Figure 29 SEM-BSE micrographs of the sample showing aggregates at 100x magnification (left) and highlighting selected areas of EDS analysis (right) 40
Figure 30 EDS microanalysis of sample CM_89 with areas highlighted in Figure 29 40
Figure 31 SEM-BSE micrographs of the sample showing a lump at 100x magnification (left) and focused on the lump at 500x highlighting selected areas of EDS analysis (right).....41
Figure 32 EDS microanalysis of sample CM_66 with areas highlighted in Figure 31 42

Figure 33 SEM-BSE micrographs of the sample showing aggregates at 100x magnification (left) and highlighting selected areas of EDS analysis (right) 42
Figure 34 EDS microanalysis of sample CM_66 with areas highlighted in Figure 34 43
Figure 35 SEM-BSE micrographs of the sample showing binder and aggregates at 100x magnification (left) and highlighting selected areas of EDS analysis (right).....43
Figure 36 EDS microanalysis of binder fraction of sample CM_76 with areas highlighted in Figure 35 44
Figure 37 EDS microanalysis of aggregate fraction of sample CM_76 with areas highlighted in Figure 35 44
Figure 38 SEM-BSE micrographs of the sample showing a lump at 100x magnification (left) and focused on the lump at 500x highlighting selected areas of EDS analysis (right).....45
Figure 39 EDS microanalysis of sample DB_V1 with areas highlighted in Figure 38 45
Figure 40 SEM-BSE micrographs of the sample showing aggregates at 100x magnification (left) and highlighting selected areas of EDS analysis (right) 46
Figure 41 EDS microanalysis of sample DB_V1 with areas highlighted in Figure 40 46
Figure 42 (a) Samples CM_70 and CM_74 (b) CONTROLS machine interface (c) CM_74 under 10 ton cell in compression (d) Compression failure of the CM_74 sample (e) CM_70 under 10 ton cell in compression (f) Compression failure of the CM_70 sample.....50
Figure 43 (a) Samples DB_v1 a & b and DB_V2 (b) DB_V1 under 2.5 ton cell in compression (c) Compression failure of the DB_V1a sample (d) Compression failure of the DB_V1b sample (e) DB_V1 under 2.5 ton cell in splitting (f) DB_V2 under 2.5 ton cell in splitting 51
Figure 44 Compressive Strength Test Results in terms of load (N) and displacement (mm) .52
Figure 45 Splitting Strength Test Results in terms of load (N) and displacement (mm) 53

List of tables

Table 1 List of all the samples taken from the Roman theater of Aquileia 13
Table 2 List of all the samples taken from the Baths of Diocletian, Rome 18
Table 3 Overview of the tests performed on each sample 19
Table 4 Samples prepared for compressive and splitting tests 25
Table 5 Sample categories defined after the optical microscopy analysis 26
Table 6 Features and characteristics of Aquileia samples analyzed by OM 32
Table 7 Features and characteristics of Diocletian baths samples analyzed by OM 34
Table 8 Samples selected for the SEM-EDS analysis 35
Table 9 Mineralogical composition of Aquileia mortar samples from XRPD analysis 48
Table 10 Mineralogical composition of Diocletian baths mortar samples from XRPD analysis 49
Table 11 Results of the compression and splitting tests 54

Acknowledgements

I would like to extend my immense gratitude and appreciation for the unwavering support and guidance I've received throughout the course of my master's degree and this dissertation.

First and foremost, I am deeply thankful to my supervisor, Prof. Michele Secco, and co-supervisor, Simone Dilaria, for their invaluable guidance, patience, support, and encouragement throughout this journey. I am equally grateful to my co-supervisors, Prof. Enrico Garbin and Dr. Valeria Razzante, whose provision of necessary resources and generous support were indispensable to the completion of this research.

I also extend my appreciation to the faculty of the Department of Geosciences, the Department of Cultural Heritage, and the members of various departments for their mentorship in this graduate program. Their collaboration and willingness to share their expertise were invaluable to this research. I would also like to acknowledge the financial support provided by the University of Padova through the Veneto Region scholarship, which made this master's degree possible for me.

I am profoundly grateful to my family and friends for their unwavering support and belief in my abilities throughout this academic journey. I would especially like to thank my late father for sowing the seed of curiosity in me and encouraging me to explore every avenue in life and education. Lastly, I extend my heartfelt thanks to my fellow ASCH students, whose camaraderie and support made this journey not only rewarding but truly memorable.

This dissertation is a culmination of the collective efforts, guidance and encouragement I have received, and for that, I am sincerely appreciative.

Ringraziamenti

Vorrei esprimere la mia immensa gratitudine e apprezzamento per il sostegno costante e la guida che ho ricevuto durante il corso del mio Master e la preparazione di questa tesi.

Prima di tutto, sono profondamente grato al mio supervisore, il Prof. Michele Secco, e al co-supervisore, Simone Dilaria, per la loro guida inestimabile, pazienza, sostegno e incoraggiamento lungo tutto questo percorso. Sono altrettanto riconoscente ai miei co-supervisori, il Prof. Enrico Garbin e Dott.ssa Valeria Razzante, il cui apporto di risorse necessarie e il generoso sostegno sono stati indispensabili per il completamento di questa ricerca.

Esprimo inoltre la mia gratitudine ai docenti del Dipartimento di Geoscienze, del Dipartimento di Beni Culturali e ai membri dei vari dipartimenti per il loro mentoring in questo programma di laurea. La loro collaborazione e disponibilità a condividere la loro esperienza sono stati inestimabili per questa ricerca. Desidero anche riconoscere il supporto finanziario fornito dall'Università di Padova tramite la borsa di studio della Regione Veneto, che ha reso possibile questo Master.

Sono profondamente grato alla mia famiglia e ai miei amici per il loro incrollabile sostegno e per la fiducia nelle mie capacità durante questo percorso accademico. Vorrei ringraziare in modo particolare il mio defunto padre per aver seminato in me il seme della curiosità e per avermi incoraggiato a esplorare ogni ambito della vita e dell'istruzione. Infine, desidero ringraziare i miei compagni di studi ASCH, il cui cameratismo e supporto hanno reso questo percorso non solo gratificante, ma veramente memorabile.

Questa tesi rappresenta la culminazione degli sforzi collettivi, della guida e dell'incoraggiamento che ho ricevuto, e per questo sono sinceramente riconoscente.

Abstract

Roman civilization is universally recognized for the development of Roman concretes which are known for their exceptional strength and mechanical properties having survived for years since the conception of numerous Roman monuments and structures. From the revival of antiquity in the renaissance era to modern day, the scholars have always posed questions spanning a wide array of topics, making up of construction techniques, the effectiveness and efficiency of these designs against time and other forces of nature. Notably, the resilience of Roman concretes, particularly Opus Caementicium, has been observed to strengthen over time.

In this study, multiple samples were selected from the Theater of Aquileia and the Diocletian baths in Rome, reflecting significant differences in composition, strength, geographical provenance, and historical periods. A multidisciplinary approach was employed to gain insight into the mechanical characterization of these samples, focusing on the relationship between material composition and mechanical properties. Analysis techniques included Optical Microscopy, Scanning Electron Microscopy with Energy-Dispersive X-ray Spectroscopy (SEM-EDS), X-ray Powder Diffraction (XRPD), and compressive and splitting strength tests.

The study highlights the importance of archaeometric characterization for understanding the technological advancements and material choices of ancient civilizations, providing valuable insights for future conservation and restoration projects.

Sommario

La civiltà romana è universalmente riconosciuta per lo sviluppo dei cementi romani, noti per la loro eccezionale resistenza e proprietà meccaniche, che hanno resistito per secoli sin dalla concezione di numerosi monumenti e strutture romane. Dal Rinascimento ai giorni nostri, gli studiosi hanno sempre posto domande su un'ampia gamma di argomenti, che comprendono le tecniche costruttive, l'efficacia e l'efficienza di questi progetti nel tempo e contro altre forze della natura. In particolare, la resilienza dei cementi romani, in particolare dell'Opus Caementicium, è stata osservata rafforzarsi nel tempo.

In questo studio sono stati selezionati vari campioni provenienti dal Teatro di Aquileia e dalle Terme di Diocleziano a Roma, che riflettono differenze significative in termini di composizione, resistenza, provenienza geografica e periodi storici. È stato adottato un approccio multidisciplinare per ottenere informazioni sulla caratterizzazione meccanica di questi campioni, concentrandosi sulla relazione tra composizione dei materiali e proprietà meccaniche. Le tecniche di analisi utilizzate includono la microscopia ottica, la microscopia elettronica a scansione con spettroscopia a dispersione di energia (SEM-EDS), la diffrazione dei raggi X in polvere (XRPD) e test di resistenza alla compressione e a trazione per spacco.

Lo studio evidenzia l'importanza della caratterizzazione archeometrica per comprendere i progressi tecnologici e le scelte materiali delle antiche civiltà, fornendo preziose intuizioni per futuri progetti di conservazione e restauro.

1. Introduction

Throughout antiquity, the Romans have enjoyed universal recognition for the remarkably well-designed and meticulously engineered structures that have endured as a long-standing legacy. These architectural marvels, ranging from grand amphitheaters to the intricate network of aqueducts supplying water to the cities, have captivated the imagination and curiosity of scholars, historians and general public alike. The sophistication, grandeur and sheer scale of the architecture and urban planning of public infrastructure demonstrate not just the wealth and power of the empire but also the skill, innovation and advanced knowledge of the engineers and architects.

Renaissance era brought to us a renewed interest in the art, culture and history of the classical antiquity, and along with it started the preliminary development of collecting and studying ancient artifacts, manuscripts and monuments, which developed over the years and formally became a part of the profession we recognize these days as archaeology.

This renewed interest in antiquity led to the rediscovery of the marvels of Roman engineering and was followed by earning the admiration of engineers, artists, and architects (Bartman, 2020). This developed not only from the curiosity and desire to understand the context of these historical structures but also from a recognition of the advanced techniques and materials employed. Modern scholars have also developed a new focal point, the structural design and materials used by the Romans.

The questions posed by these modern scholars span a wide array of topics, making up of construction techniques, the effectiveness and efficiency of these designs against time and other forces of nature. The resilience of these materials, particularly the concretes that we know as *Opus Caementicium*, has been found to have strengthened over time.

The answer to these questions largely lies in a combination of factors including the use of strong and durable materials, the exceptional workmanship quality into every aspect of the construction and the extensive research into the repair and renovation techniques. Studying these ancient structures on the modern day is a very helpful tool to gain insights into architecture and engineering that can be implemented on the contemporary architecture and engineering and carrying forward the lessons of the past into the future.

With this thesis project, we undertook a detailed investigation into the structural properties and composition of Roman concretes, focusing on samples from the Theater of Aquileia and the Diocletian Baths in Rome. We conducted research following a systematic approach, beginning with a thorough literature review of historical and contemporary studies on Roman

concrete technology. This was followed by a series of material analyses using Optical Microscopy, Scanning Electron Microscopy with Energy-Dispersive X-ray Spectroscopy (SEM-EDS), and X-ray Powder Diffraction (XRPD) to characterize the microstructure and mineral composition of the samples. Additionally, we conducted mechanical testing, including compressive and splitting strength tests, to evaluate the performance of these ancient materials.

These methods were conducted not only from the perspective of understanding the durability of Roman concretes but also for gaining insight into conservation and restoration of historical monuments in the future.

1.1. Research Objectives

The main interest of this research project is to focus on the material composition of the Roman concretes from the sites of the Diocletian baths in Rome and the Theatre of Aquileia to parametrize their mechanical and compositional characteristics. The aim is to identify the composition of the binders and explore potential variations in the raw materials used, in addition to examining the chemical compositions and the implications on the mechanical properties of the mortars. To do so, four different analyses were employed to conduct investigations on the samples prepared using diverse methods. The tests performed include X-Ray Powder Diffraction (XRPD), Polarized-Light Optical Microscopy (OM), Scanning Electron Microscopy couples with Energy-Dispersive X-Ray Spectroscopy (SEM-EDS) and Mechanical Strength Tests (compression and splitting).

2. *Opus Caementicium*

Roman concrete, also known as *Opus Caementicium*, is considered one of the most notable feats of engineering from the antiquity period. The discovery of this revolutionized the design and construction of structures and was widely employed in Roman architecture. Made of a mixture of lime (Calcium oxide), water, pozzolana (volcanic ash), and aggregates (stones or brick fragments etc.), *opus caementicium* is not equivalent to contemporary concrete which employs the use of Portland cement with aggregate sizes smaller than the ones used in antiquity. It's widely regarded that it derives its strength from the use of pozzolana, a fine volcanic ash that imparted remarkable strength and longevity to the concrete due to the pozzolanic reactions.

The term Pozzolan in modern day refers generally to any kind of amorphous silicate compound employed in cement production processes, however the name is derived from Puteoli, a roman city in the bay of Naples where volcanic ash was exploited as *pulvis puteolanus* (Dilaria, et al., 2023).

Pozzolanic mortars are different from aerial lime binders due to the reaction between calcium from the lime and the pozzolan's amorphous silicate (Secco, et al., 2018; Dilaria et al. 2023). These mortars can consistently set in humid environments as well due to the requirement of water for the pozzolanic reactions, even when permanently submerged. The pozzolanic materials aren't strictly volcanic in origin. Crushed ceramics and organic ashes were also used often as they were rich in silicates and an accessible alternative to volcanic materials in case of geological unavailability of natural volcanic pozzolans. Crushed ceramics used in this case were referred to as *coccio-pesto*, which were versatile in use and often employed in brickmaking and pottery industry as well (Moropoulou, et al., 1995). Therefore, the pozzolanic materials utilized by the romans can commonly be categorized into 3 types: geological, ceramic-base and organic-derived.

The other major reactive substance in *opus caementicium* is calcium hydroxide, also referred to as slaked lime. In antiquity, slaked lime production was a largescale industry as it is crucial for both structural mortars and surface plasters. The slaked lime production in antiquity was done by firing geological calcite in a kiln to a temperature above 700 degrees Celsius, ideally up to 900 degrees. In this process, calcium carbonate (mainly mineral calcite, $CaCO_3$) is transformed into quicklime (CaO) while Carbon dioxide (CO_2) is released. The quicklime is subsequently powdered by crushing and mixed with water to create slaked lime ($Ca(OH)_2$)

(Secco, et al., 2020). In typical aerial lime binders, the slaked lime is allowed to dry. When the water vaporizes to escape, the system absorbs ambient carbon dioxide, reforming calcite:

Carbonate rock + Heat → Quicklime + Carbon Dioxide

$$CaCO_3 + \Delta E \rightarrow CaO + CO_2$$

Quicklime + Water → Slaked Lime + Heat

$$CaO + H_2O \rightarrow Ca(OH)_2 + \Delta E$$

Slaked Lime + Atmospheric Carbon Dioxide → Calcite + Water

$$Ca(OH)_2 + CO_2 \rightarrow CaCO_3 + 2H_2O$$

In Pozzolanic mortar production, the slaked lime is mixed with pozzolan and water. When saturated in a highly alkaline mixture of slaked lime, pozzolans start dissolving and form Calcium-Silicate-Hydrate (C-S-H) around their external perimeter (Barnes and Benson 2002). This outer shell eventually bursts under the pressure from osmosis allowing the entire pozzolanic particle to dissolve and reach with calcium hydroxide. C-S-H is a chain silicate with greater strength than the calcite in aerial lime mortars, and it is fortified by additional products like Calcium-Aluminum-Hydrates (C-A-H, sometimes also referred to as AFm due to their Aluminum and Iron content). This continues until either the reactants or the water are consumed completely.

Slaked Lime + Alumina-Silicate + Water → Calcium Silicate Hydrate + Calcium Aluminate Hydrate

$A = Al_2O_3$, C= CaO H= H_2O, S = SiO_2

CH + AS + H → C-S-H + C-A-H

Opus Caementicium is only one among many other construction materials and techniques employed during the Roman era. It was often used as foundation for construction of monumental structures, and its plasticity and waterproof properties made it ideal for use in thermal complexes. This mixture of mortar, fine sands and coarse aggregates solidifies as a result of the pozzolanic reactions, thus creating artificial monolith structures. It represents most of the samples extracted from both the sites, Roman theater of Aquileia and Diocletian baths in Rome in the form of foundations, thick walls and the mortar between bricks that acted as the formwork for pouring the *opus caementicium*.

3. Historical context of the sites

The two sites chosen for our research project represent completely different time periods of execution and geographical provenance of the pozzolanic material, which enables us to see the stark difference in the development of construction techniques and materials between the two eras and the effect of the pozzolanic aggregates used on the mechanical characteristics of the structures over the years.

3.1. Roman Theater of Aquileia

Aquileia was one of the main Roman towns of the ancient Cisalpina region (modern day Northern Italy) established as a colony in 181 BCE in an inland area of Friuli lowland. Strategically positioned along the Natisone River, approximately 10km from the Adriatic Sea, it served as an important crossroad for trade routes connecting the Roman empire to various territories. The strategic location of the colony contributed to the rapid growth of Aquileia as a commercial and military hub with monumental buildings and prestigious houses, reflected in its rich archaeological record. In a historical inscription (*Ordo urbium nobelium*, IX) CE Ausonius mentioned it as one of the largest cities in the Roman world.

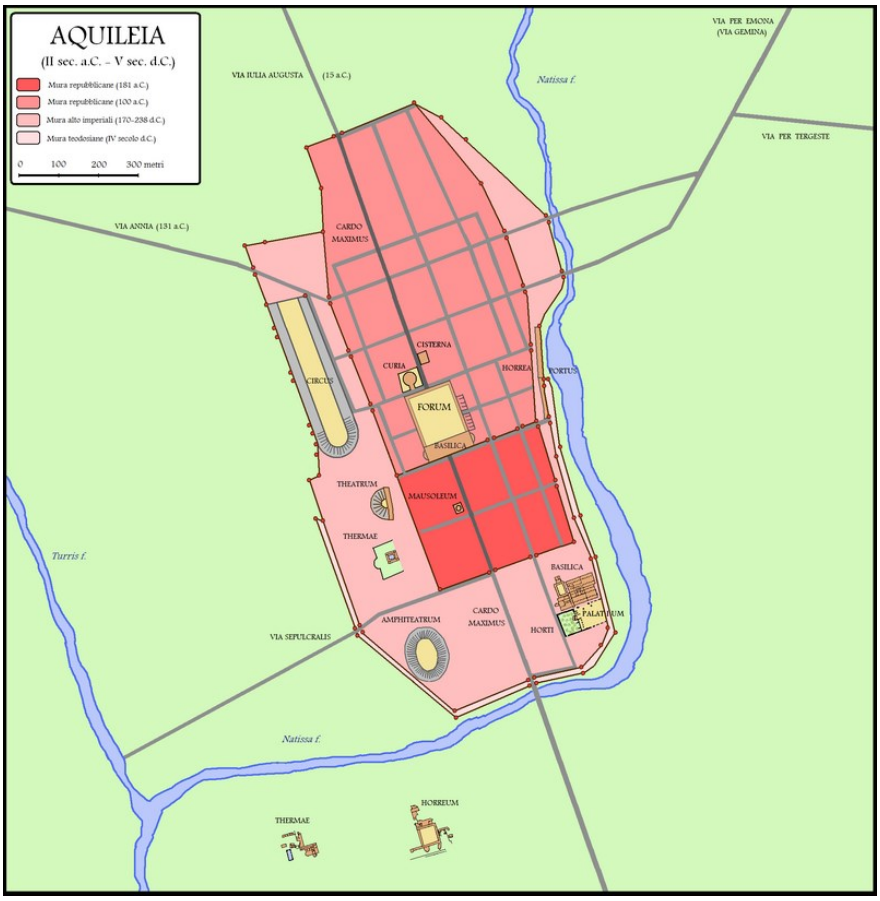

Figure 1 Ancient Roman city of Aquileia

Archaeologically, it is considered one of the most important Roman sites in Northern Italy. Excavation work executed in the past has revealed an elaborately planned city with a typical Roman style grid layout featuring a forum, basilica, baths, temples and a network of roads and aqueducts (Rubinich, et al., 2024).

Among the many notable structures in Aquileia, the theater is a key monument reflecting the cultural and social dynamics of the city during the Roman period. Indicative of the Roman emphasis on public entertainment and social cohesion, the structure was built in the first century CE. It features an elliptical arena for spectacles that was integral to Roman public life and tiered seating to accommodate the spectators.

Some of the most significant information for the research was made available in the 2018-2019 excavation period and helped with the identification of planimetric and architectural definition of the building. The most important being the identification of the entrance of the theatre facing north and a significant part of the relative access corridor, and the completion of the study of orchestra and transversal investigation of the entire stage building along the median axis of the theatre (Ghiotto, et al., 2021).

The existence and approximate location of the Roman theater within the urban plan of Aquileia was suggested by archaeologist Luisa Bertacchi in the past decade. The exact location was revealed by the excavation activities carried out by the University of Padova since 2015, identifying its proximity to the urban forum and outside the republican walls of the city. The results of these excavations were detailed plans, orientation, dimensions and building techniques of the theater spanning across a diameter of approximately 95m, making it one of the largest Roman theaters in the *Cisalpina* region, along with theaters of Pola, Padova and Verona (Ghiotto, et al., 2021).

The structure was built in a low-lying land which was possibly riddled with the problem of water infiltration like the entire city of Aquileia in the antiquity. This demanded a solution in the form of a sufficiently consolidated foundation, which was realized with the help of an *Opus Caementicium* foundational substructure divided into three concentric sectors, each corresponding to the tiers of the steps, the *summa*, *media* and *ima cavea* (Figure 7). The overall layout, architectural design elements and initial studies of the site suggest that the theater was built at the beginning of the 1st c. CE (Dilaria, et al. 2023).

The theater, with its use of local materials and accommodating the landscape, offers valuable insights into Roman construction techniques especially the development of Roman

concrete recipes. Through the careful analysis of the samples from the site, we can identify how the materials employed have contributed to the structural strength over the centuries.

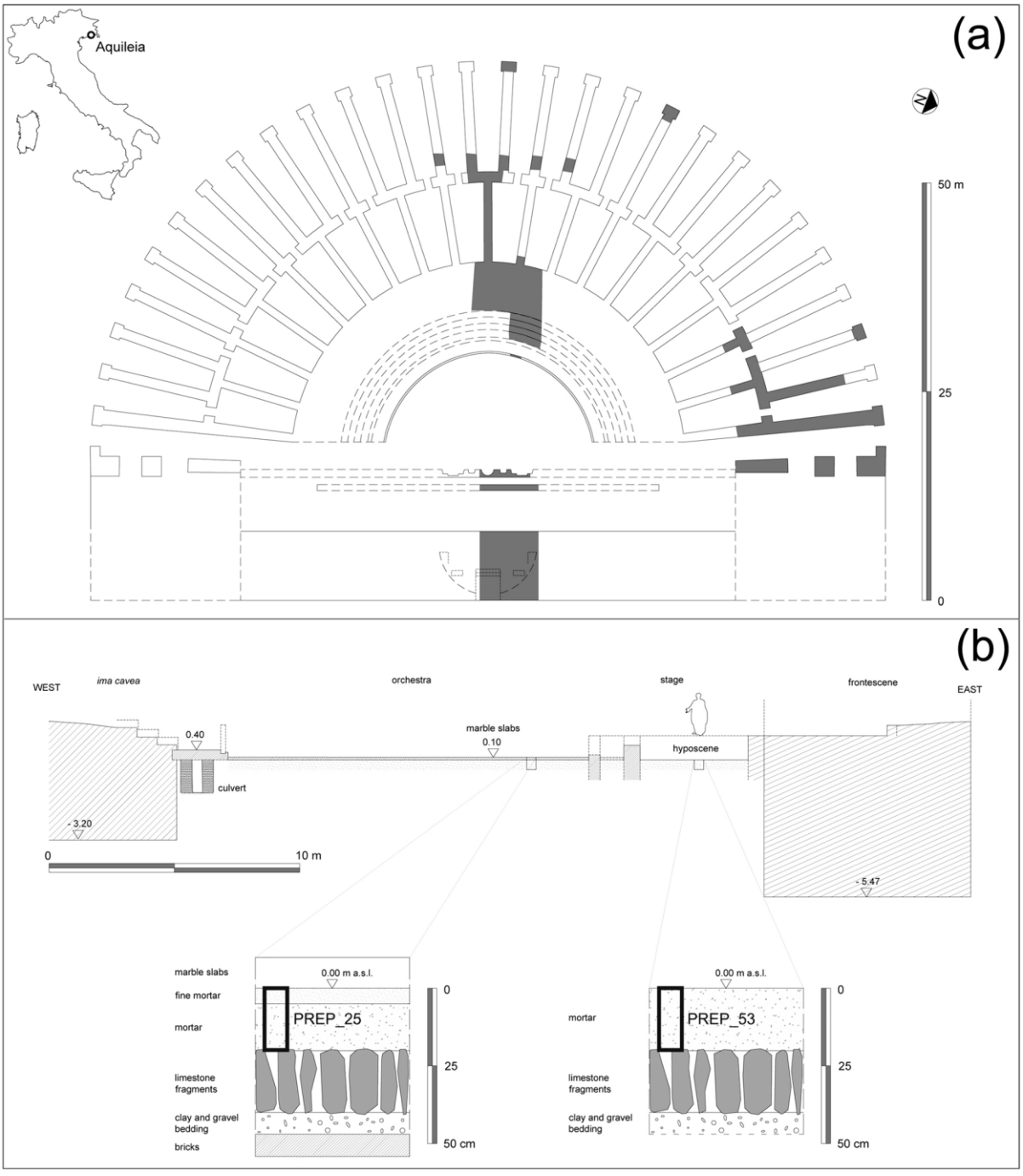

Figure 2 The Roman theatre in Aquileia. (a) Reconstructive plan of the building with indication of the excavated sectors (in dark grey); (b) Reconstructive cross section of the theatre, from the ima cavea to the scaenae frons wall, with stratigraphic sketches of the floor preparations of the orchestra and hyposcaenium. (Source: Dilaria et al. 2023)

3.2.Diocletian Baths, Rome

The Diocletian baths (Latin: Thermae Diocletiani, Italian: Terme di Diocleziano) were public baths in ancient Rome. Built between 298 to 306 AD and named after the emperor Diocletian, they were the largest of the imperial baths.

Figure 3 Baths of Diocletian, with the basilica of Santa Maria degli Angeli e dei Martiri built in the remains of the baths

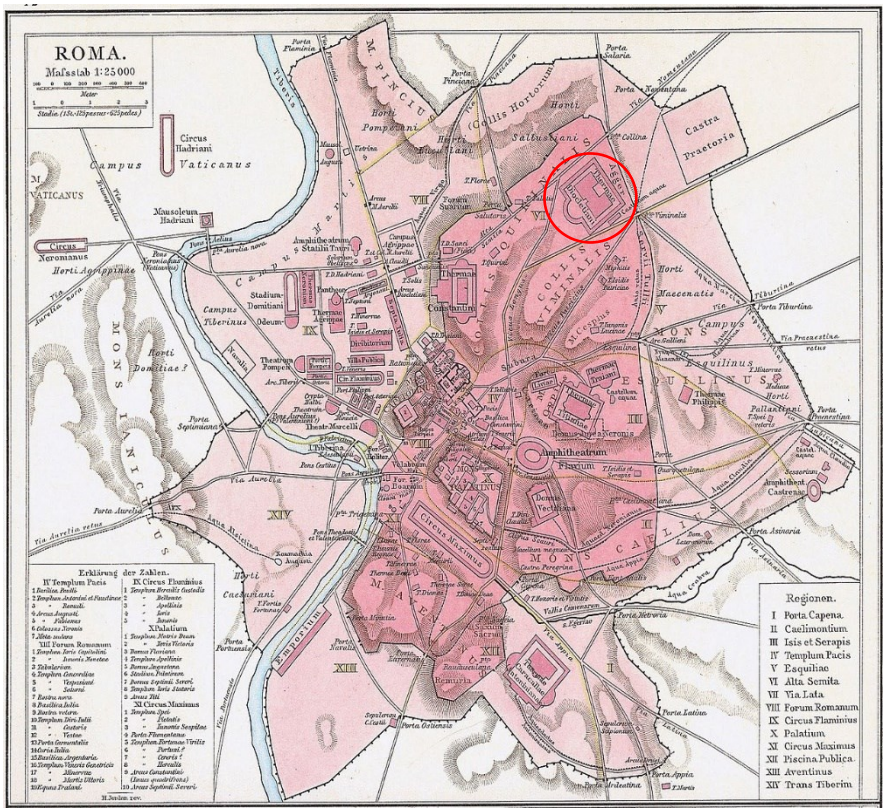

Figure 4 The location of the baths in Rome during Antiquity

The baths were commissioned by Maximian in honor of co-emperor Diocletian in 298 AD. Evidence certifying the validity of this can be found in bricks from the main area of the baths, which bear stamps of the Diocletianic period. The construction of the complex continued from the year it was commissioned until the abdication of Diocletian in 305 and the demise of Constantinus in 306. (Platner and Ashby 1929)

The bath complex spanned over an area of thirteen hectares (32 acres), comparable to the baths of Caracalla. The central block consisted of *frigidarium* (cold baths), *tepidarium* (thermal room), and *caldarium* (hot baths) along a single axis. The *frigidarium* was flanked by two open air gymnasiums, while the *caldarium* was flanked by two octagonal halls.

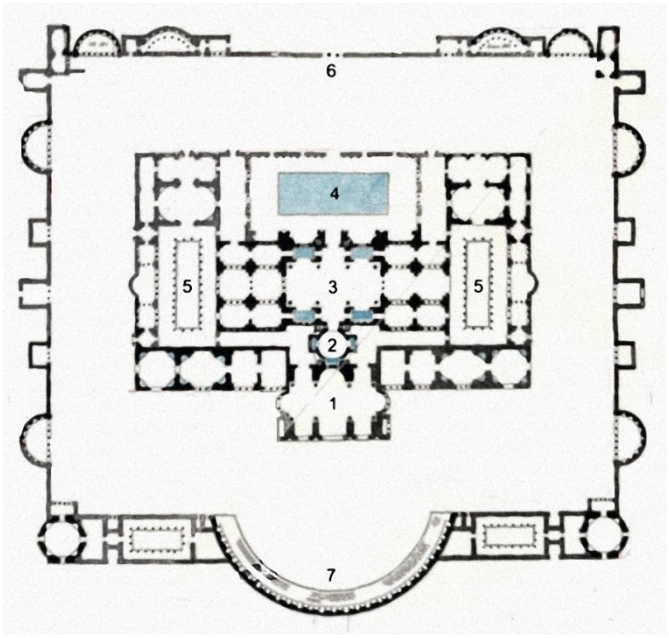

Figure 5 Reconstructed floorplan:(1) Caldarium, (2) Tepidarium, (3) Frigidarium, (4) Natatio, (5) Palaestra, (6) main entrance, (7) Exedra

The baths underwent a restoration in the early 5th century and remained in use until the siege of Rome in 537, when the aqueducts to Rome were disrupted by the king Vitiges of Ostrogoths. The medieval guidebook "*Mirabilia Urbis Romae*" refers to the bath complex as "Palatium Diocletiani".

In the 1560s, Pope Pius IV commissioned a basilica in the remains of the baths, as a commemoration of Christian martyrs who died during the construction of the baths according to legends, the basilica of Santa Maria degli Angeli e dei Martiri (Plevoets and Van Cleempoel, 2019). Michelangelo was commissioned with the task of designing the basilica, which he undertook using the *frigidarium* and *tepidarium* structures of the baths. The main cloister of the church was planned inside the Carthusian charterhouse also commissioned by the Pope.

Michelangelo achieved a sequence of shaped architectural spaces with a dominant transept, developed from a Greek cross, with cubic chapels at each end, and the effect of a transverse nave. (Ackerman 1961) The basilica doesn't have a facade, but a simple entrance marked by its unique concave brick form which was originally one of the ancient exedras of the *caldarium* of the bath complex. The rest of the bath complex was converted into grain and oil stores of the city of Rome after 1575 under the Pope Gregory XIII.

Figure 6 The church facade: an apse in the wall of the caldarium of the Baths of Diocletian

Once Rome became a part of the Kingdom of Italy, the seat of the government was moved to the city. In 1884, the charterhouse was abandoned by the Carthusians and the areas around the baths underwent significant changes including the construction of Roma Termini station, the Grand Hotel and Palazzo Massimo. Gaetano Koch designed the palazzi in the facing the Piazza dell'Esedra (now Piazza della Repubblica) destroying a part of the porticos. The western gymnasiums were cut off from the rest of the enclosure by Via Cernaia and are now located in Via Parigi. In 1889, the Italian government set up the Museo Nazionale Romano in the baths and inside the charterhouse.

The Diocletian baths stand, with the extensive use of local bricks and concrete, particularly the development and application of *opus caementicium* using the local volcanic tuffs for building massive vaulted halls and structures, demonstrate the ability of the Romans to construct large open structures with durability, strength and longevity, ensuring the stability of the vast structures over the centuries. By analyzing the samples from the site, we can identify how the materials evolved over the decades and how the recipes developed by the Romans have enabled the structure to withstand the passage of time while maintaining the outstanding mechanical strength and resilience.

4. Sites & Samples

From both the sites of our research focus, a total of 16 samples were selected for the analysis, comprising of 10 samples from the Roman theater of Aquileia and 6 samples from the basilica of Santa Maria degli Angeli e dei Martiri in Diocletian baths. These samples include core drills from the foundations, walls, and mortar samples from both sites.

4.1. Roman Theater of Aquileia

The abbreviation CM stands for the samples collected from the site of the buried Roman amphitheater in Aquileia, extracted with the help of rotational drills. The sampling activity on the theater site was carried out by Geoalpina S.r.l in collaboration with the University of Padova in June 2021. (Figure 7, 8 and 9). Table 3 describes the samples acquired from the site.

Figure 7 Sampling activities at the Roman theater of Aquileia

Figure 8 Location of the site and sampling points from the geognostic survey campaigns of June 2021 (Source: Geoalpina S.r.l.)

Table 1 List of all the samples taken from the Roman theater of Aquileia

Sample	Description	Function	Relative Height (m from the ground)	Location	Cores
CM_65	*Coccio-pesto* mortar	Structural – Lowest foundational layer for waterproofing	-5.60/.65	Saggio 4  S1 C2	
CM_66	*Coccio-pesto* mortar	Structural – Lowest foundational layer for waterproofing	-6.00/.10	Saggio 4  S1 C2	
CM_69	Tough lime mortar	Structural – Lowest foundational layer for waterproofing	-6.00/.20	 S2 C2	
CM_70	Lime mortar	Structural – Upper foundational layer core drill	-3.62/.80	 S3 C1	
CM_74	Very tough lime mortar	Structural – Upper foundational layer core drill	-5.00/.25	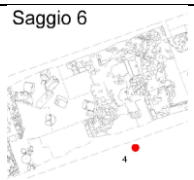 S4 C2	

CM_76	Very tough lime mortar	Structural – Upper foundational layer core drill	-7.20/.35	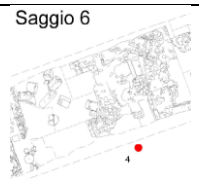 S4 C2	
CM_85	*Coccio-pesto* mortar	Structural – Archaeological layer – From the E edge of scenae frons			
CM_88	Lime mortar	Structural – Archaeological layer – Mortar from scenae frons			
CM_89	*Coccio-pesto* mortar	Structural – Archaeological layer – Wall on the western limit of scenae frons (masonry)			
CM_91	Lime mortar	Structural – Archaeological layer– Wall on the western limit of scenae frons (foundation)			

Figure 9 Core drills from the foundational layer with sampling points and their relative heights

4.2.Diocletian Baths, Rome

The abbreviation DB on the other hand lists the samples extracted from the pillars inside Diocletian baths and is further categorized into C and V. The samples with letter C correspond to core drills from the nucleus of the *opus caementicium*, while the letter V correspond to micro cores for stratigraphic analysis. The sampling activity on this site was carried out by SO.IN.G. strutture e ambiente S.r.l. in 2022. (Figure 9 and 10)

Figure 10 Sampling process at the Basilica of Santa Maria degli Angeli (Source: SO.IN.G. strutture e ambiente S.r.l.)

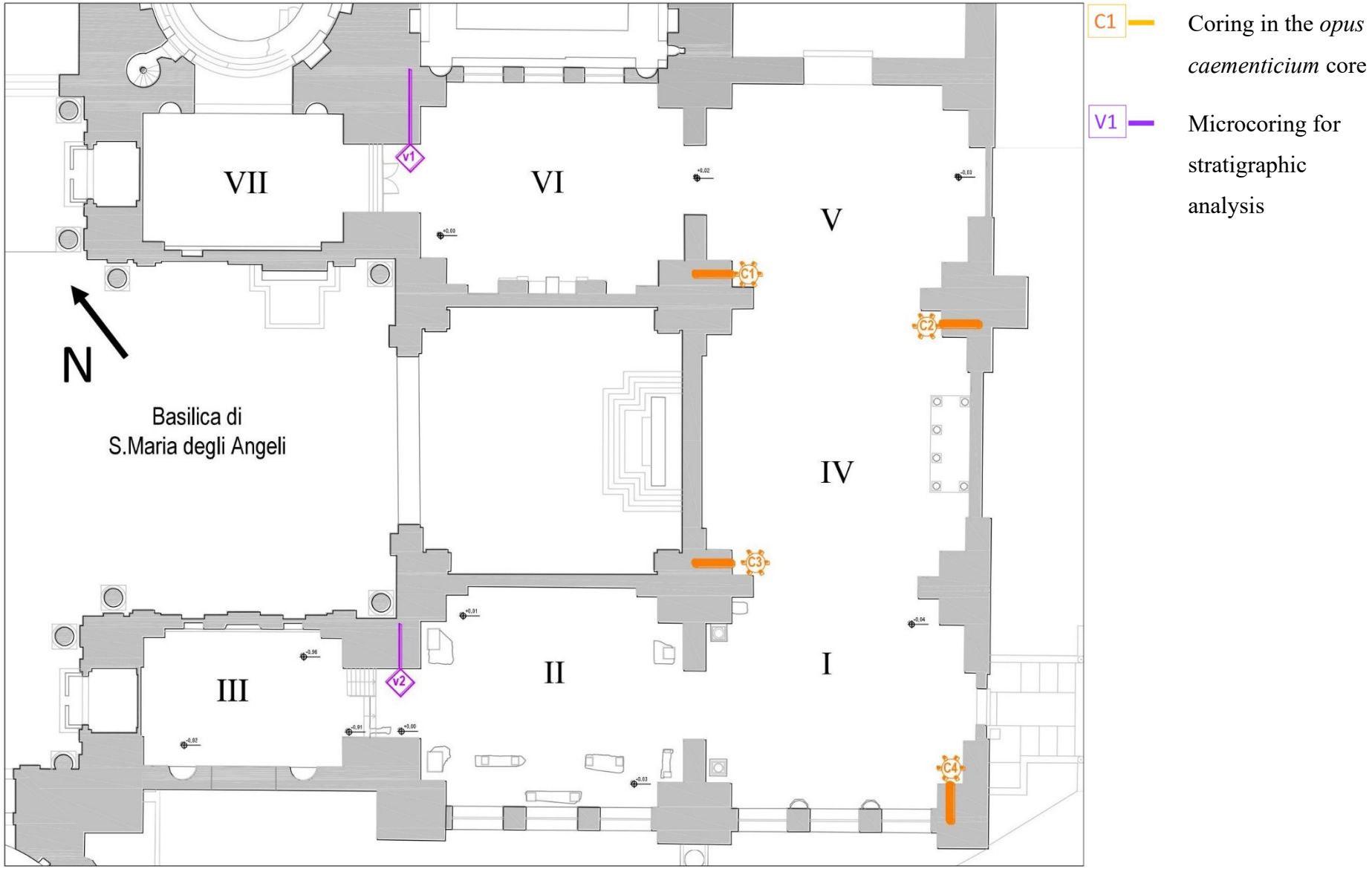

Figure 11 Location of the cores inside the Baths of Diocletian, Rome (Source: SO.IN.G. strutture e ambiente S.r.l.)

Table 2 List of all the samples taken from the Baths of Diocletian, Rome

Sample	Chronology	Function	Location	Cores
DB_C1	4th Century Roman	Structural – Nucleus of load bearing columns	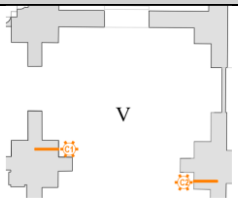	
DB_C2	4th Century Roman	Structural – Nucleus of load bearing columns	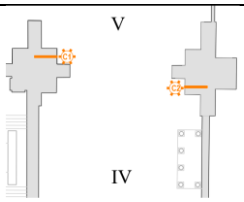	
DB_C3	4th Century Roman	Structural – Nucleus of load bearing columns	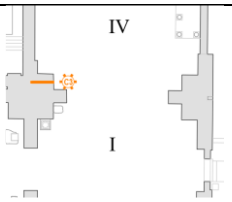	
DB_C4	4th Century Roman	Structural – Nucleus of load bearing columns	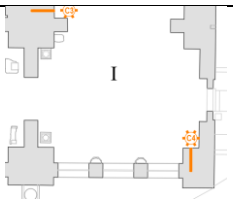	
DB_V1	4th Century Roman	Structural – Stratigraphic cores of columns	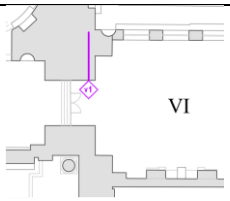	
DB_V2	4th Century Roman	Structural – Stratigraphic cores of columns	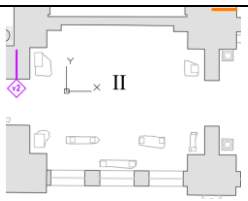	

5. Materials & Methods

Most of the samples underwent the Optical microscopy and XRPD analysis, however, due to groups of samples sharing similarities, it was decided to focus only on one representative sample of each category for SEM-EDS. For the mechanical tests, only a few samples were chosen as well due to the integrity of the cores making most of them not suitable for compression and splitting tests. Table 10 represents a list of all the samples and the analysis methods performed on them.

Table 3 Overview of the tests performed on each sample

	TL-OM	**XRPD**	**SEM-EDS**	**Mechanical tests**
Type	**Thin section**	**Powder**	**Thin section**	**Cylinder**
CM_69	X	X	X	
CM_88	X	X		
CM_91	X	X		
CM_85	X	X		
CM_89	X	X	X	
CM_70	X	X		X
CM_65	X	X		
CM_66	X	X	X	
CM_74	X	X		X
CM_76	X	X		
DB_C1	X	X		
DB_C2	X	X		
DB_C3	X	X		
DB_C4	X	X		
DB_V1	X	X	X	X
DB_V2	X			X

5.1. Optical Microscopy

All sixteen samples from both the sites were analyzed in the form of thin sections with a Leica DM7500 P polarized light microscope incorporating a set of objectives with magnification ranging in 1.6x, 2.5x, 4x, 10x. Thin sections of 30 microns thickness were

studied without reference to the sampling map to ensure minimal bias in grouping decisions. Digital micrographs of the samples were also captured with the help of an integrated digital camera FLEXACAM C1. All the petrographic analysis were performed at the Department of Cultural Heritage of the University of Padova.

Thin sections of ~30 μm were obtained by vacuum-impregnating portions of the materials with epoxy resin. The preparation of a thin section for optical microscopy involves a meticulous and systematic process to ensure the sample's suitability for detailed microscopic examination. Below is a brief description of the steps undertaken to prepare these samples.

Initially, a representative portion of the sample is selected ensuring that it is both dry and clean. The sample then undergoes cutting using a diamond saw (we used the Struers Labotom-3 to perform this step). The cut surface must be smooth and flat; therefore, it undergoes polishing with the help of a machine and/or manually if needed. In our preparation, it was done using Struers LaboPol-5 followed by manual polishing on a glass plate using 300 grit silicon carbide and water. The cut and polished surface is then cleaned and mounted onto a glass slide with the help of epoxy resin ensuring that it is firmly attached and level with the epoxy. It is then allowed to be cured completely which may take several hours to overnight depending on our choice of resin. Once the curing process is finished, excess material is trimmed away.

The next phase of this process involved grinding the sample to gradually reduce its thickness. This was done using progressively finer abrasive discs or paper, starting with coarse grits and moving to finer ones. The thickness was checked regularly to ensure it reached 100 microns. Once this thickness was achieved, the samples were polished further with very fine abrasives like aluminum oxide or diamond paste until the standard thickness of about 30 microns was reached. This final thickness allows for optimal light transmission during optical microscopy.

After the polishing stage, the thin sections undergo a meticulous cleaning to remove any remaining compound or debris using distilled water and a soft brush or ultrasonic cleaner. The section is then labeled with any pertinent information such as sample name, date etc. using a permanent marker, printed label for clarity and durability.

5.2. XRPD

All sixteen samples of the mortars were analyzed using XRPD. The constraints on choosing the material to grind involved a selection of representative pieces of the sample. The preparation of the samples for the analysis was performed in the laboratories of the Department of Geosciences at the University of Padova.

Each sample was coarsely ground with a hammer in a closed container to produce millimeter sized particles. The powder was then ground further using a mortar and pestle to achieve approximately 500 microns diameter before micronizing the sample with a McCrone XRD-mill. The process of micronizing with the McCrone XRD-mill was done in the following phases:

- A plastic tube with zirconia grinding elements is cleaned from any remaining residue by micronizing only with 15ml of water for two minutes. This is repeated twice to ensure removal of all residues.
- After rinsing the tube with the zirconia elements, a small fraction of the sample and 15ml of ethanol is added to it and micronized for five minutes in the mill.

The micronizing leaves us with a slurry of our micronized sample and ethanol which is then poured onto a glass dish and left to dry overnight. Upon drying, the dry powder is scraped off the container and weighed. For our analysis, 0.8 g of sample powder was mixed with 0.2 g of zinc oxide (ZnO) to obtain a 1 g mixture. The addition of zinc oxide is helpful for understanding composition of sample and detecting the amorphous content. This mixture of sample and zinc oxide is once again inserted into a mortar and pestle to ensure a cohesive mixing of the fine powders.

Finally, the powder is mounted onto the zero-background sample holders using backloading technique to offset the potential of preferred orientation of crystals present in the sample.

Grinding the samples into fine powders is extremely effective for XRPD analysis as it helps to improve the random orientation of the crystals. The prepared samples are processed by diffracting the x-ray across the faces of each crystal and capturing the pattern by a detector (Moropoulou et al. 1995). Most minerals have defined patterns and atomic structures.

The analysis was performed using Bragg–Brentano θ-θ diffractometer (PANalytical X'Pert PRO, Cu Kα radiation, 40 kV and 40 mA) equipped with a realtime multiple strip (RTMS) detector (Malvern PANalytical, Malvern, UKPIXcel by Panalytical). The data acquisition was

done by continuous scanning from the angles 4–85 (◦2θ) for regular samples and 4-89 (◦2θ) for micro-samples with a virtual step scan of 0.02 (°2θ). The mineral phases were then identified using the PDF database references with the help of Malvern Panalytical's software X'Pert HighScore Plus. Further quantitative analysis was performed by Rietveld refinement using Bruker's Topas DiffracPLUS software, retrieving structural data from the International Crystal Structure Database (ICSD).

Figure 12 Philips X'Pert PRO diffractometer, Bragg-Brentano geometry with Bragg-Brentano HD optics, cobalt source, X'Celerator detector, and Anton Paar HTK16 hot stage. (source: https://www.geoscienze.unipd.it/diffrattometria-x-polveri)

A drawback of using XRPD is that it relies on crystalline structures to reflect the x-rays from all possible crystal surfaces. Due to the amorphous nature of pozzolans and C-S-H, they won't be registered by the detector. However, the addition of zinc oxide (ZnO) as a standard is useful for allowing us to calculate the unmeasured fraction of the amorphous phases later.

5.3.SEM-EDS

Scanning electron microscopy and Energy dispersive X-ray spectroscopy (SEM-EDS) was chosen to analyze the microstructural and microchemical characteristics of the mortars. Four samples were analyzed using this technique including two samples representative of the two groups and an outlier among the Aquileia samples, while one representative sample from the Diocletian baths ones was analyzed.

SEM utilizes the secondary electrons expelled from the outer shells of atoms to construct a morphological view of the analyzed objects up to a nanometric scale. (Owsiak, 2024) SEM-BSE (Backscattered electrons) analysis on the other hand follows the beam-generated electrons

and interprets the elastic interaction between the beam and sample by monitoring the intensity of reflected electrons through a sensor. The EDS (Energy dispersive spectrometer) provides a partial quantifiable composition of selected areas or points on the sample.

As mentioned in Table 1, the technique was applied on thin sections previously mentioned in Section 5.1. The 30-micron thin section requires additional polishing to be suitable for SEM-EDS analysis. This was done using a Struers LaboPol-35 in the Department of Geosciences at the University of Padova. Additionally, a layer of nanometric gold was applied to induce a higher electrical conductivity to optimize the scanning and microanalysis.

The SEM-EDS analysis was performed with COXEM EM-30AX scanning electron microscope at CEASC laboratory of the University of Padova. It is equipped with a tungsten filament, a solid type 4-channel BSE detector, and an energy dispersive X-ray detector (EDX) EDAX Element-C2B. For the analysis of thin sections and imaging the analytical working conditions were the following: accelerating voltage 20kV; filament current 1.80A; emission current 20μA; aperture current 300nA; working distance 20-30mm.

Figure 13 COXEM EM-30AX Tabletop SEM with STEM detector at Insertion position using the side accessory port

The sample analysis was performed at various magnifications and indirect images were acquired to highlight areas of interest in the mortars, particularly reaction edges and lumps of mortar. After performing the SEM-EDS analysis, concentrations of the major elements Al, Fe, Si, Ca, and Mg were determined by analyzing selected areas of the binder.

5.4.Mechanical Tests

The difficulty of working with archaeological mortars stems from the irregularity of the samples and therefore the unreliability with standardized mechanical testing procedures (Velosa et al., 2010). The samples acquired from our selected sites also presented the same problem due to the state of integrity and sizes of most samples therefore the mechanical testing was limited to 2 core drills from the Aquileia samples and the 2 micro-cores from Diocletian baths. These samples were chosen on the basis of the state of integrity and the suitability of the dimensions for the testing.

Uniaxial compression tests and splitting tests (also known as Brazilian tests) were carried out according to the main principles of standards EN 12390-3[1] and EN 12390-6[2]. For the cylindrical samples, we calculated the mean diameter at mid-height in the central area where uniaxial fracture occurs (Panizza et al., 2020). Three diameter measurements were taken at 120° intervals. Similarly, three height measurements were taken at 120° intervals. The surface area in contact with the press was also calculated for all the samples to set the machine's analysis parameters.

The top and bottom surfaces of all samples were covered with a cement cap to ensure proper contact with the steel plates of the machine and prevent uneven loading from the machine. The maximum load was recorded for calculating compressive strength f_c (Equation 1), were P_{max} is the failure load, and A_c is the cross-sectional area of the specimen on which the compressive force acts. Splitting strength "f_{sp} was calculated according to Equation 2, where d and L are the average diameter and length in correspondence of the diametral plane under loading.

[1] EN 12390-3. Testing Hardened Concrete-Part 3: Compressive strength of test specimens. European Committee for Standardization (2011).
[2] EN 12390-6. Testing Hardened Concrete-Part 6: Tensile splitting strength of test specimens. European Committee for Standardization (2000).

$$f_c = \frac{P_{max}}{A_c} \quad (1)$$

$$f_{sp} = \frac{2 \cdot P_{max}}{\pi \cdot L \cdot d} \quad (2)$$

Table 2 outlines the properties of the selected samples: diameter, height, weight, area, and apparent density.

Table 4 Samples prepared for compressive and splitting tests

Sample	ϕ (mm)	h (mm)	Weight (g)	Area (mm2)	Density (g/cm3)
CM_70	84.67	157.33	1520	5630.08	1.716
CM_74	87.50	186.67	2520	6013.20	2.245
DB_V1a.comp	27.73	39.00	41.93	604.08	1.780
DB_V1b.comp	27.80	39.70	43.79	606.99	1.817
DB_V2.comp	27.73	38.40	40.31	604.08	1.738
DB_V1.split	27.80	16.10	15.14	606.99	1.549
DB_V2.split	27.60	16.30	15.05	598.28	1.543

6. Results

This chapter presents a thorough analysis and interpretation of the findings from the tests performed on a total population of 16 samples as described in table 1. These methods were utilized to characterize and identify mineralogical compositions, chemical and mechanical properties of our samples, and highlight the most important findings of each analysis.

6.1. Optical Microscopy

The petrographic analysis of the thin sections from Aquileia revealed variation in composition, and therefore the samples were divided into three main categories: Lime mortars with sand & gravel (Group 1), *Coccio-pesto* mortars with pluri-millimetric ceramic fragments (Group 2) and *Coccio-pesto* mortars with ceramic fragments and fine dust (Group 3). Additionally, an outlier was defined (Lime mortar with fragments of limestone and no sand). On the other hand, the six samples from Diocletian baths presented a very similar composition and therefore were grouped altogether. Table 5, reported below, refers to the samples corresponding to the groups defined during the petrographic analysis.

Table 5 Sample categories defined after the optical microscopy analysis

Group		**Samples**
Aquileia	Group 1: Lime mortars with sand & gravel	CM_69
		CM_88
		CM_91
	Group 2: *Coccio-pesto* mortars with ceramic fragments	CM_70
		CM_85
		CM_89
	Group 3: *Coccio-pesto* mortars with ceramic fragments and terracotta dust	CM_65
		CM_66
	Outlier: Lime mortar with fragments of limestone and no sand	CM_76
Diocletian Baths		DB_C1
		DB_C2
		DB_C3
		DB_C4
		DB_V1
		DB_V2

6.1.1. Aquileia

Group 1: Lime mortars with sand & gravel

Group 1 contains 3 samples from two structures: CM_69, CM_88 and CM_91. This group is distinguishable by the presence of sand & gravel within the calcic lime binder. (Figure 14)

The group is characterized by high birefringence within the micritic binder matrix except for one sample CM_69, showing zoning of areas with low & high birefringence. This zoning is potentially caused by the development of hydrated phases in the matrix. Lime lumps are present in all 3 samples in a very small amount. The samples are marked by relatively low number of voids, mostly vughs and a small amount of channels.

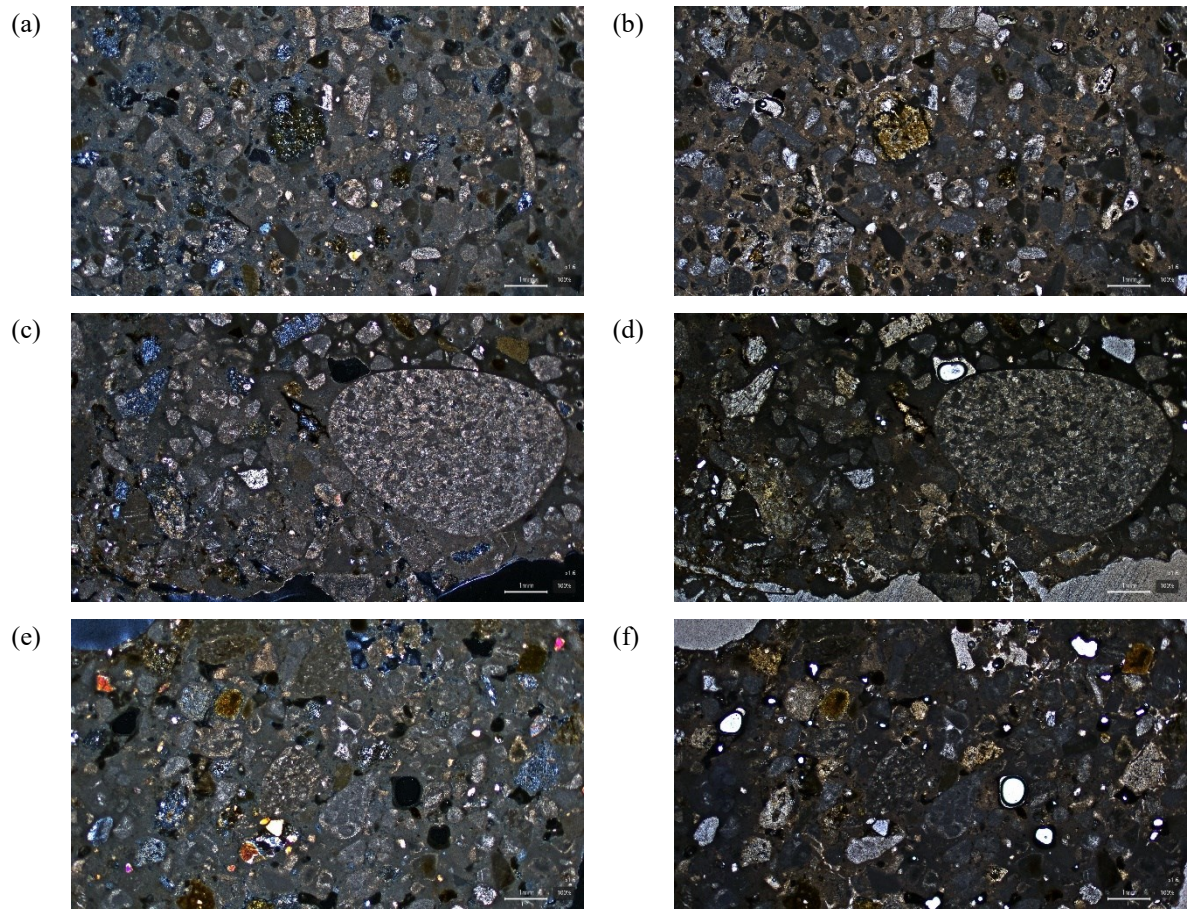

Figure 14 Micrographs of Group 1 samples showing general composition: CM_69, CM_88 and CM_91 under plain polarized light (a, c & e) and cross polarized light (b, d & f) 1.6x magnification (Scale bar: 1mm)

The samples are marked by the presence of aggregates mostly from the very coarse sand class, except sample CM_91 which is from the very fine gravel class, according to Wentworth scale. (Wentworth, 1922) The majority of clasts are rounded, and the samples

present a small amount of angular clasts as well, which refers to the mechanical fragmentation of carbonate and limestone elements as a way of recycling building materials. Rare ceramic fragments were detected, likely recycled bricks. Overall, the distribution between coarse and fine aggregates is well balanced, with an even distribution throughout the matrix.

Regarding the petro-mineralogical composition, the aggregates are composed of carbonate clasts of limestone and dolostone, followed by subordinate concentration of quartz, chert and scattered sandstones. Sample CM_91 also presents a small fraction of cherty limestones fragments. In the sample CM_69, the carbonate clasts, particularly dolomitic aggregates, exhibit strong reaction edges (Figure 15) and ghosts of dolostone as a result of the de-dolomization process. (Katayama 2010) The same sample also exhibits strong reactions of chert aggregates and ghosts of chert marked by defined reaction edges. Sample_88 includes a very small quantity of clay pellets as well. Sample CM_69 also exhibits a small inclusion of post-depositional pyrite (Secco, et al., 2018).

(a) 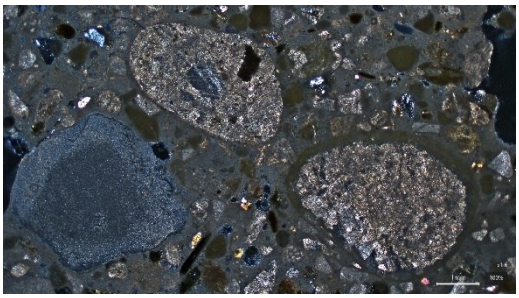 (b) 

Figure 15 Sample CM_69 showing micrographs of dolomitic aggregate exhibiting clear reaction edges in (a) plain olarized light and (b) cross polarized light 1.6x magnification (Scale bar: 1mm)

Group 2: *Coccio-pesto* mortars with ceramic fragments

Group 2 contains 3 samples from two structures: CM_70, CM_85 and CM_89. (Figure 16) This group is distinguishable due to the relevant presence of ceramic fragments in the matrix. However no ceramic dust was detected. This group is characterized by samples showing zoning of areas with high and low birefringence (primarily low) except CM_89 which only exhibits low birefringence. This zoning is potentially caused by variation of the distribution of hydrated phases. The high birefringence indicates zones with good carbonation. The samples are primarily micritic but CM_85 and CM_89 present zones of sparitic texture as well. The samples contain very few lumps. The voids are fairly low in frequency and are mostly vughs with a small amount of cracks present in the samples CM_70 and CM_89.

A characteristic of this group is the presence of coarse sub-centimetric ceramic fragments. Overall, the distribution between coarse and fine aggregates is well balanced with an even distribution throughout the matrix.

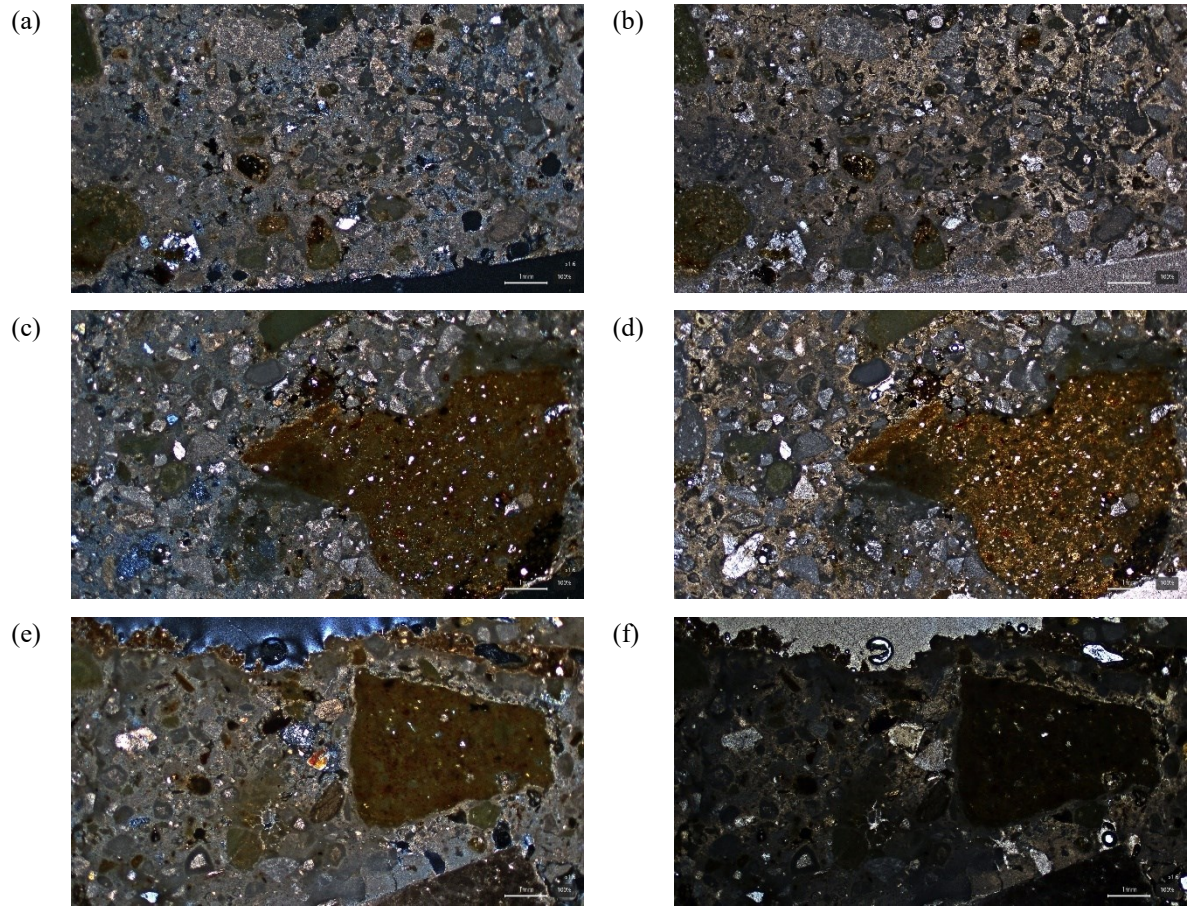

Figure 16 Micrographs of Group 2 samples showing general composition: CM_70, CM_85 and CM_89 under plain polarized light (a, c & e) and cross polarized light (b, d & f) 1.6x magnification (Scale bar: 1mm)

Regarding the mineralogical composition, the sandy component is made of carbonate clasts of limestone and dolostone, quartz, and chert. Samples CM_70 and CM_89 also show a very minute amount of limestone chips and fragments while CM_85 shows reused clasts of mortar signifying the recycling of building materials. Sample CM_89 also exhibits slight reactions of brick fragments and dolomitic aggregates however they are not developed as detected in CM_69. (Figure 17)

(a)  (b) 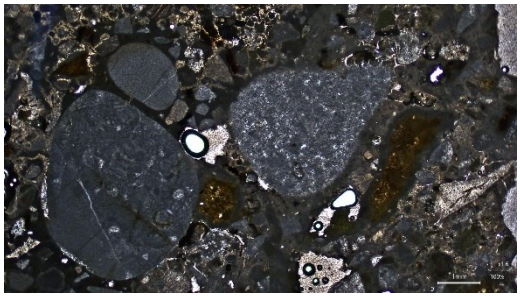

Figure 17 Sample CM_89 showing micrographs of dolomitic aggregates and brick fragments exhibiting clear reaction edges in (a) plain polarized light and (b) cross polarized light 1.6x magnification (Scale bar: 1mm)

Group 3: *Coccio-pesto* mortars with ceramic fragments & terracotta dust

Group 3 contains 2 samples from the same structure: CM_65 and CM_66. This group is distinguishable by the presence of ceramic dust, which was not present in group 2, along with the presence of coarse ceramic fragments. (Figure 18)

This group is characterized by samples showing primarily low birefringence, however CM_65 also presents zones of high birefringence. The high birefringence indicates good carbonation of the binder. The samples are micritic in texture and exhibit lumps in a moderate amount. They also show a moderate amount of voids that are equally represented in the form of vughs and cracks.

The ceramic fragments represent the largest aggregate type of Group 3. Subordinately, a sandy component of the same petro-mineralogical composition and grain size of samples of groups 1 and 2 was detected. Overall, the distribution between coarse and fine aggregates is fairly to moderately good. Sample CM_66 is homogenous, while CM_65 is heterogenous with improper mixing of ceramic powder into the mortar.

Sample CM_66 exhibits secondary calcite presence along the pores due to prolonged exposure to the water circulation, possibly determined by its location in the foundational layers of the theatre related to the action of groundwater intrusion.

(a) 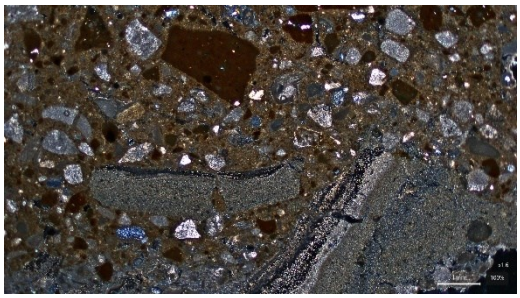 (b) 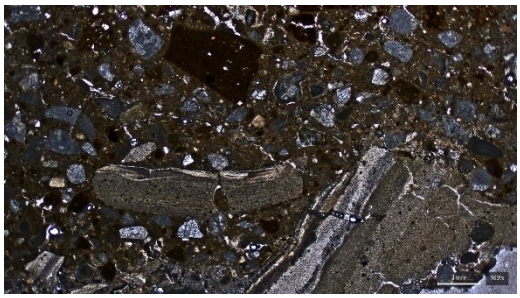

(c) 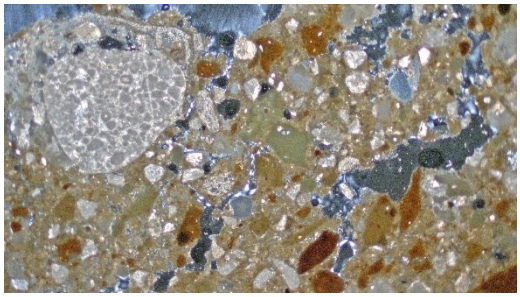 (d) 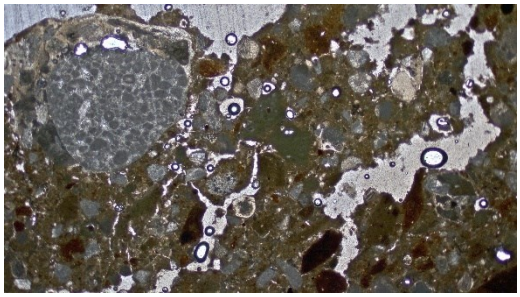

Figure 18 Micrographs of Group 3 samples showing general composition: CM_65 and CM_66 under plain polarized light (a & c) and cross polarized light (b & d) 1.6x magnification (Scale bar: 1mm)

Outlier: Lime mortar with fragments of limestone and no sand

CM_76 is the sole outlier of this study. The matrix is micritic and homogeneous, with high birefringence. The sample is moderately porous, showing voids in the form of vughs and cracks. Overall, the distribution between coarse and fine aggregate is well-balanced.

The main type of aggregate is constituted by limestone fragments, possibly originating from the Karst area. Chert and carbonate clasts of limestone and dolostone are present in small quantities. Quartz and ceramic fragments are sporadic.

(a) 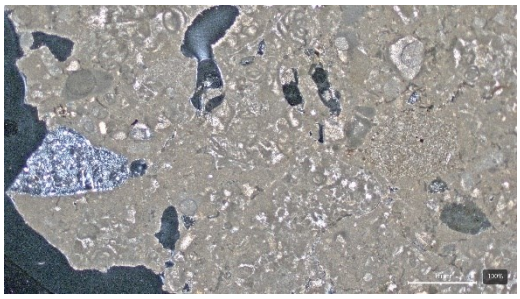 (b) 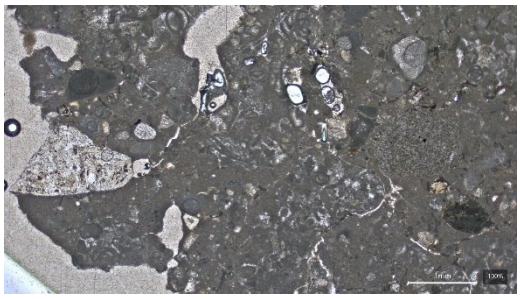

Figure 19 Micrographs of CM_76 showing general composition under plain polarized light (a) and cross polarized light (b) 1.6x magnification (Scale bar: 1mm)

Table 6 Features and characteristics of Aquileia samples analyzed by OM

Group	Sample	Binder		Voids		Aggregate														
		Type	Lumps amount	Types	Overall amount	Carbonatic clasts	Chert	Cherty limestone	Quartz	Brick powder	Ceramic fragments	Iron oxides	Lime fragments	Shell	Feldspar	Clay pellets	Reused coccio pesto mortar	Max grain size (µm)	Min grain size (µm)	Mean grain size (µm)	Standard deviation	Wentworth size class
Group 1: Lime mortar (Sand/Sand with gravel)	CM_69	Calcic micritic	+	Vughs, Cracks	+	+ + +	-		-		-	- -						3928.5	403	1128.4	816.0	Very Coarse Sand
	CM_88	Calcic micritic	-	Vughs, Cracks	+	+ + +	+ +		- -		- -	- -			- -	- -		6577.1	421.4	1871.6	1820.8	Very Coarse Sand
	CM_91	Calcic micritic	-	Vughs, Cracks	+	+ + +	+	-	- -		- -	- -						11656.9	446.4	2002.0	2430.1	Very Fine Gravel
Group 2: Coccio Pesto with brick fragments, no dust	CM_70	Calcic micritic	-	Vughs, Cracks	+ +	+ + +	-		-	+	-	- -	-					10061.4	447.8	1693.5	905.8	Very Coarse Sand
	CM_85	Calcic sparitic to micritic	-	Vughs	-	+ +	-		+	- -	+						- -	4103.9	565.2	2548.7	2087.5	Very Fine Gravel
	CM_89	Calcic sparitic to micritic	-	Vughs, Cracks	+ +	+ +	-		-		+ +	- -	- -	- -				4344.1	460.1	1622.7	1160.2	Very Coarse Sand
Group 3: Coccio Pesto with a lot of terracota dust	CM_65	Calcic micritic	+	Vughs, Cracks	+ +	+	-		-	+	+ +							5864.1	378	1793.1	1603.8	Very Coarse Sand
	CM_66	Calcic micritic	-	Vughs, Cracks	+	+	-		-	+ +	+ +	- -						5140.4	266	1115.6	1137.4	Very Coarse Sand
Outlier	CM_76	Calcic micritic		Vughs, Cracks	+	-	-		- -		- -		+ + +					3863.1	183.6	1050.9	964.7	Very Coarse Sand

6.1.2. Diocletian Baths

All 6 samples from the Diocletian baths were grouped together as they exhibited very similar compositions.

The samples are characterized by variable birefringence within the microsparitic binder matrix, while samples DB_C1 and DB_C4 show relevant zoning with areas of low and high birefringence. Lime lumps are present in a very small quantity. The samples are marked by relatively low to moderate amount of voids in the form of vughs. (Figure 20)

The samples are marked by the presence of aggregates mostly from thev very coarse sand class, except DB_C3 which shows aggregates in coarse sand class, (Wentworth, 1922) in the form of volcanic pozzolanas, primarily constituted by Pozzolane Rosse from the Colli Albani (Marra et al., 2015). A subordinate concentration is represented by Volcanic tuffs, recurring in a small amount in all samples. Sample DB_C1 also exhibits scattered negative traces of fiber inclusions in the matrix. Overall, the distribution between coarse and fine aggregates is very good with an even distribution throughout the matrix.

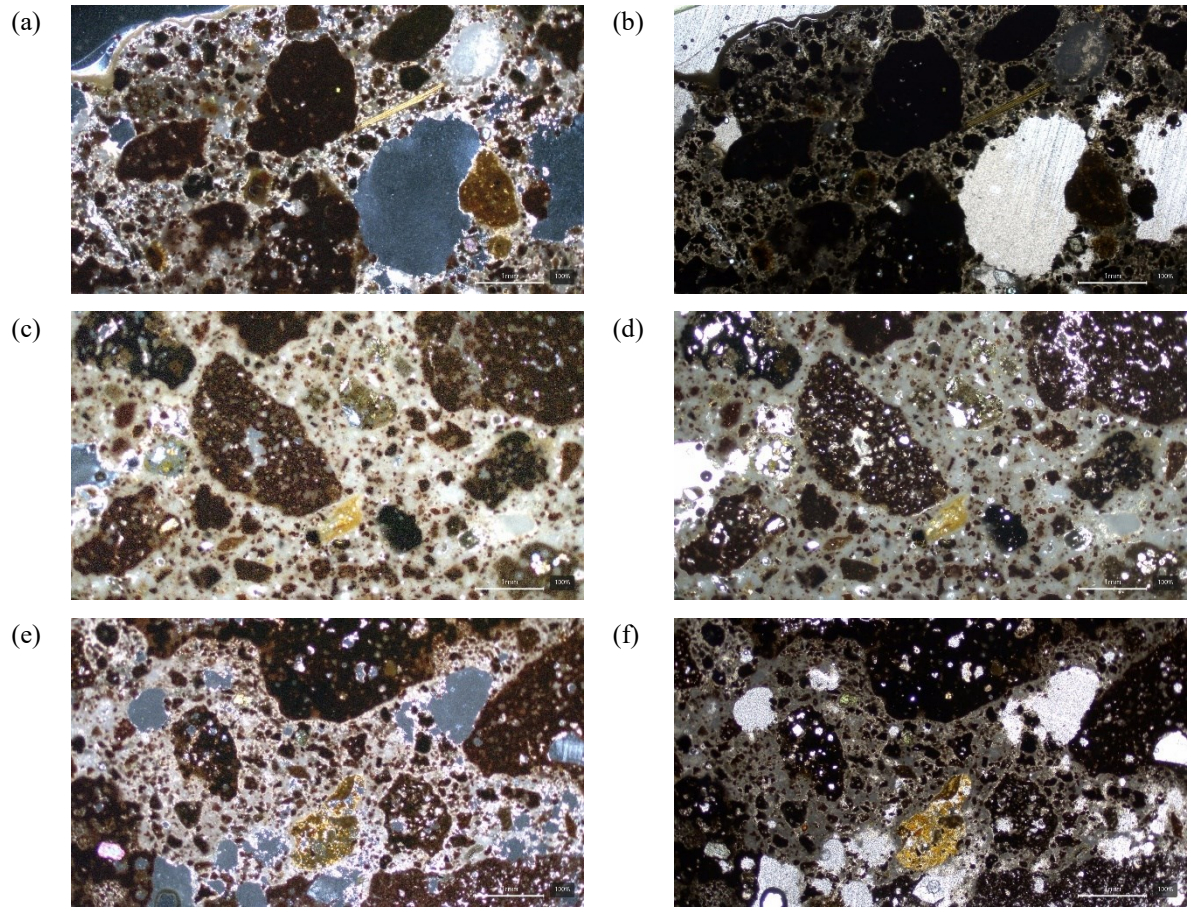

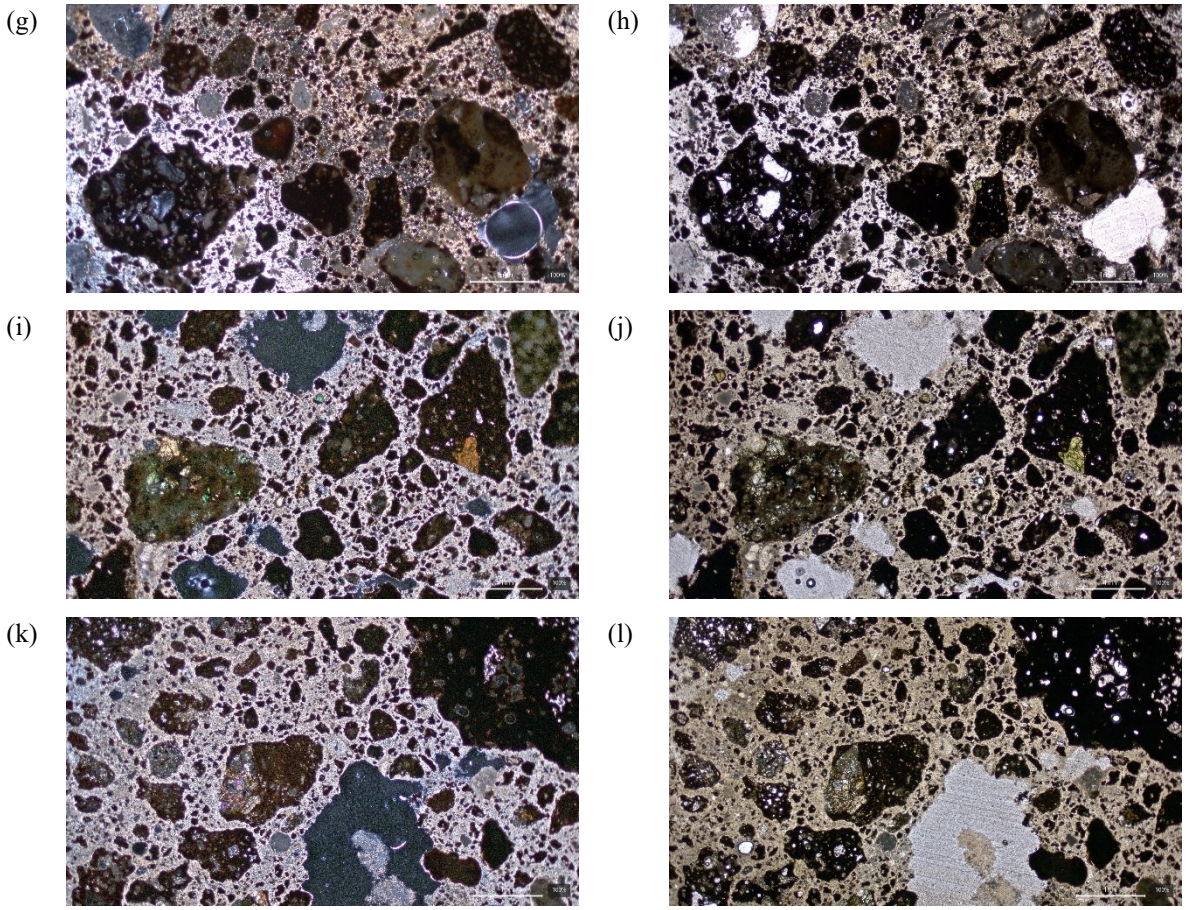

Figure 20 Micrographs of Diocletian baths samples showing general composition: DB_C1, DB_C2, DB_C3, DB_C4, DB_V1 & DB_V2 under plain polarized light (a, c, e, i & k) and cross polarized light (b, d, f, j & l) 1.6x magnification (Scale bar: 1mm)

Table 7 Features and characteristics of Diocletian baths samples analyzed by OM

Sample	Binder		Voids		Aggregate							
	Type	Lumps amount	Types	Overall Amount	Pozzolane (Rosse)	Volcanic Clasts/Tuffs	Fiber Inclusions	Max grain size (µm)	Min grain size (µm)	Mean grain size (µm)	Standard deviation	Wentworth size class
DB_C1	Microsparitic	-	Vughs	-	+ + +	-	- -	4833.6	369.1	1228.0	1054.7	Very Coarse Sand
DB_C2	Microsparitic		Vughs	-	+ + +	-		4400.9	352.2	1388.5	1007.8	Very Coarse Sand
DB_C3	Microsparitic	- -	Vughs	+	+ + +	-		1925.3	287.7	881.0	427.1	Coarse Sand
DB_C4	Microsparitic	-	Vughs	-	+ + +	-		2521.5	304.6	1111.3	587.4	Very Coarse Sand
DB_V1	Microsparitic	-	Vughs	+	+ + +	-		4409.7	298.7	1279.5	1021.2	Very Coarse Sand
DB_V2	Microsparitic	-	Vughs	+	+ + +	-		5002.5	246.8	1412.6	1075.4	Very Coarse Sand

6.2.SEM-EDS

The initial analysis with Optical microscopy helped us identify the major groups of samples and key topics of further investigation. For the SEM-EDS analysis, we chose one sample from each group to understand the composition of the matrix and specific aggregates, the presence of lime lumps and the reaction edges of aggregates in the samples.

The selected samples from each group are described in table 8.

Table 8 Samples selected for the SEM-EDS analysis

Group		Selected Samples
Aquileia	Group 1: Lime mortars with sand & gravel	CM_69
	Group 2: *Coccio-pesto* mortars with ceramic fragments	CM_89
	Group 3: *Coccio-pesto* mortars with ceramic fragments & terracotta dust	CM_66
	Outlier: Lime mortar with fragments of limestone and no sand	CM_76
Diocletian Baths		DB_V1

6.2.1. Group 1: CM_69

The binder fraction of CM_69 presents present high percentages of Ca, Mg and Si. The Mg:Ca:Si ratio can be attributed to the formation of C-S-H and M-S-H phases. This is consistent with the observations made based on optical microscopy. The presence of calcium can also represent an aerial lime reaction leading to the formation of calcite. (Figure 21 and 22)

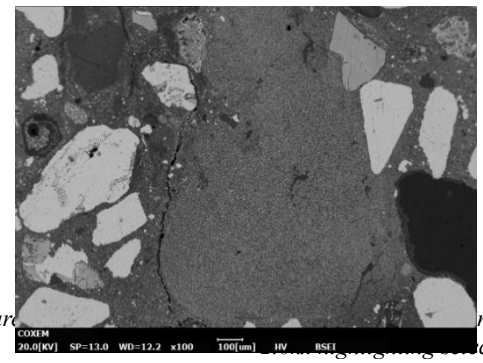

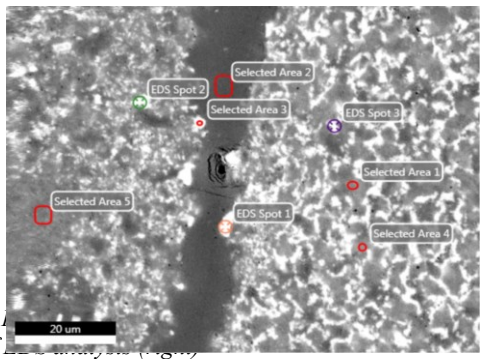

Figur ng a lump at at ected areas of

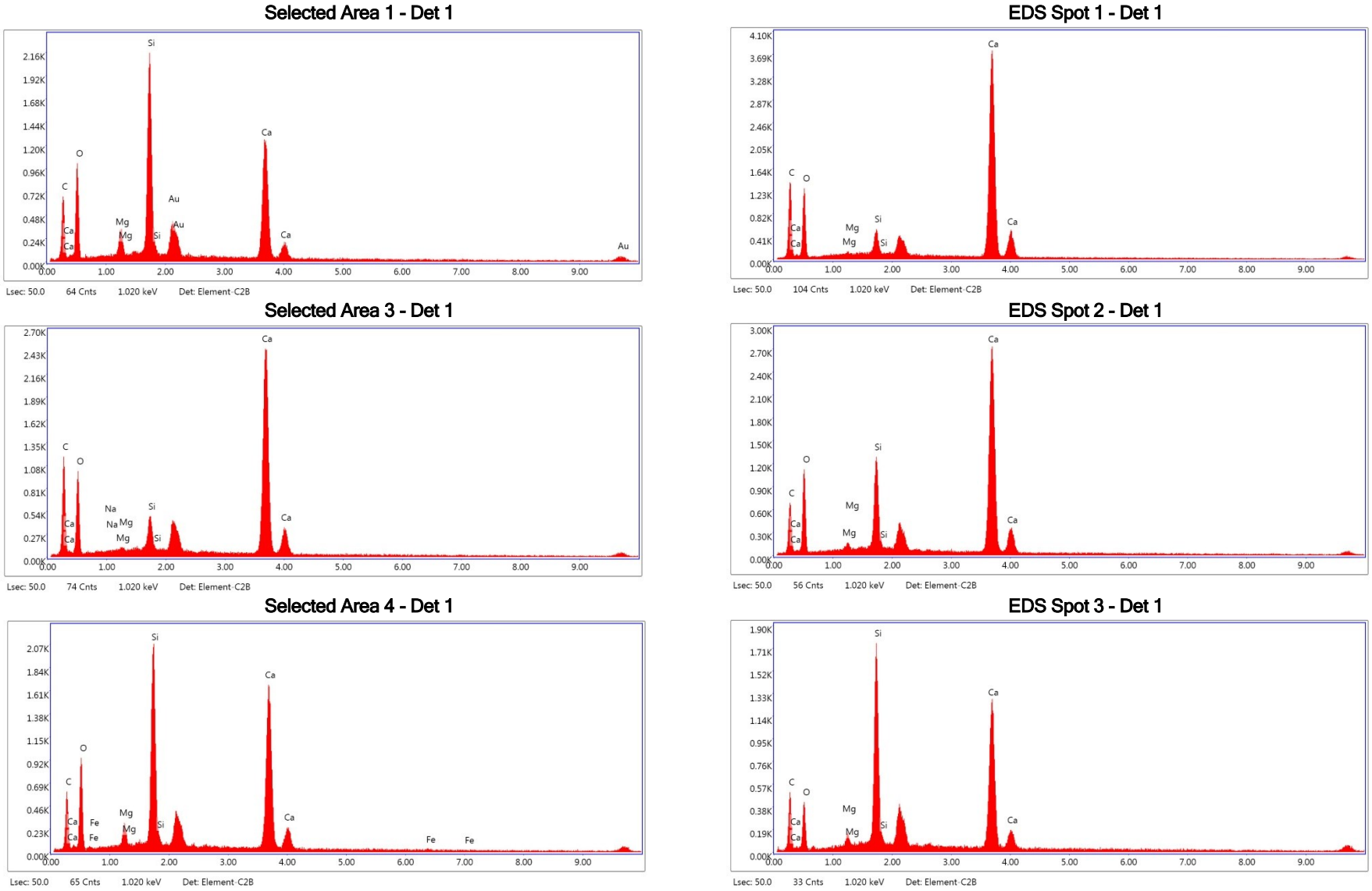

Figure 22 EDS microanalysis of sample CM_69 with areas highlighted in Figure 21

Another feature of particular interest in the sample is the presence of clear and well-defined reaction edges indicating a reaction between the binders and aggregates. This is especially noticeable for some coarse carbonate clasts in the sample. The point analyses taken in the unreacted part of the aggregate show significant peaks of Si along with small peaks of Al. This can be attributed to the observation made in the optical microscopy analysis showing reaction edges around the chert aggregates. (Figure 23)

The areas inside the reaction edges show similar peaks of Si and Al, along with the presence of peaks of Mg, C and O, which can be attributed to the reaction of binder with the chert aggregates to form M-S-H phases. The spots taken outside the reaction edges correspond to that of the binder fraction. (Figure 24)

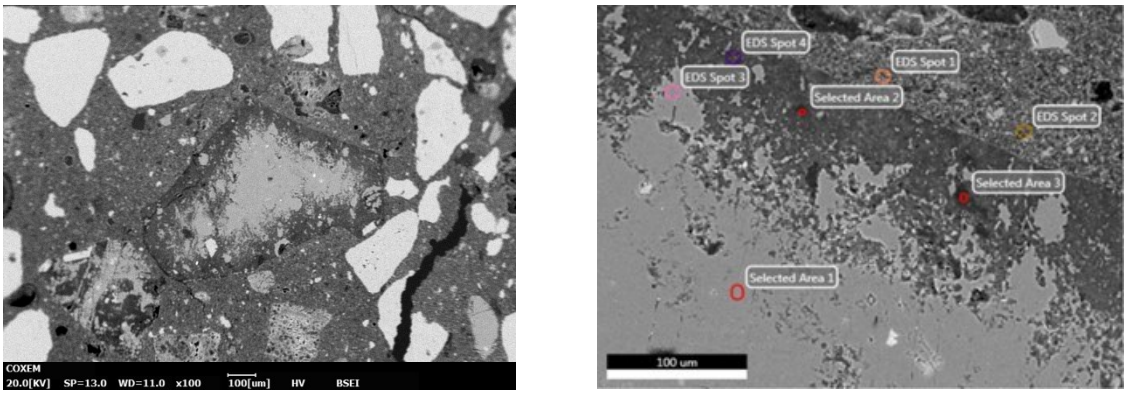

Figure 23 SEM-BSE micrographs of the sample showing a chert aggregate with reaction edges at 100x magnification (left) and focused on the reaction edge at 500x highlighting selected areas of EDS analysis (right)

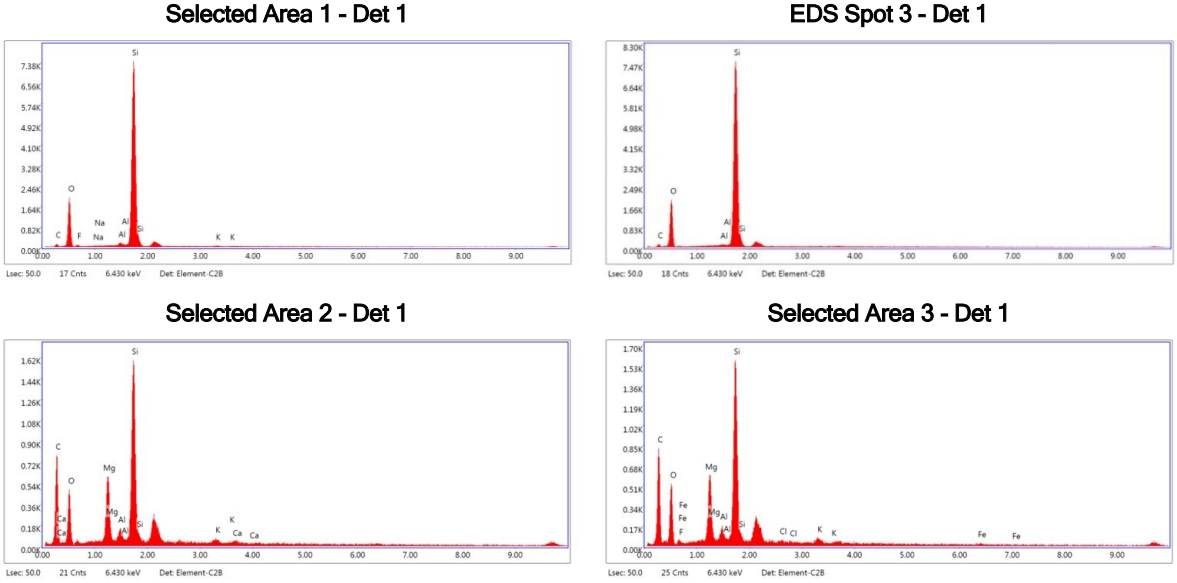

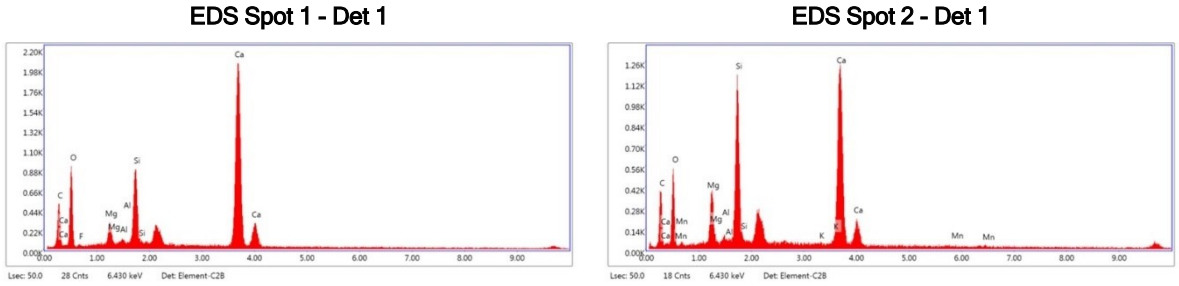

Figure 24 EDS microanalysis of sample CM_69 with areas highlighted in Figure 23

The aggregate fraction of the sample shows variations in the intensity of peaks for Mg, Si and Ca. with minor peaks of Al. This is in accordance with the observations made with the optical microscopy and XRPD analysis showing calcium silicate minerals or magnesium silicate minerals, commonly found in binding composites rich in dolostone. (Figure 25 and 26)

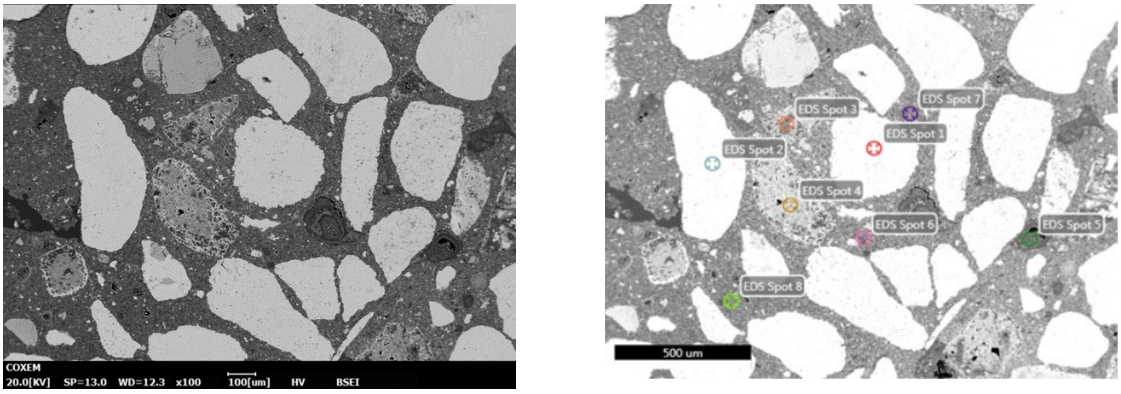

Figure 25 SEM-BSE micrographs of the sample showing a chert aggregates at 100x magnification (left) and highlighting selected areas of EDS analysis (right)

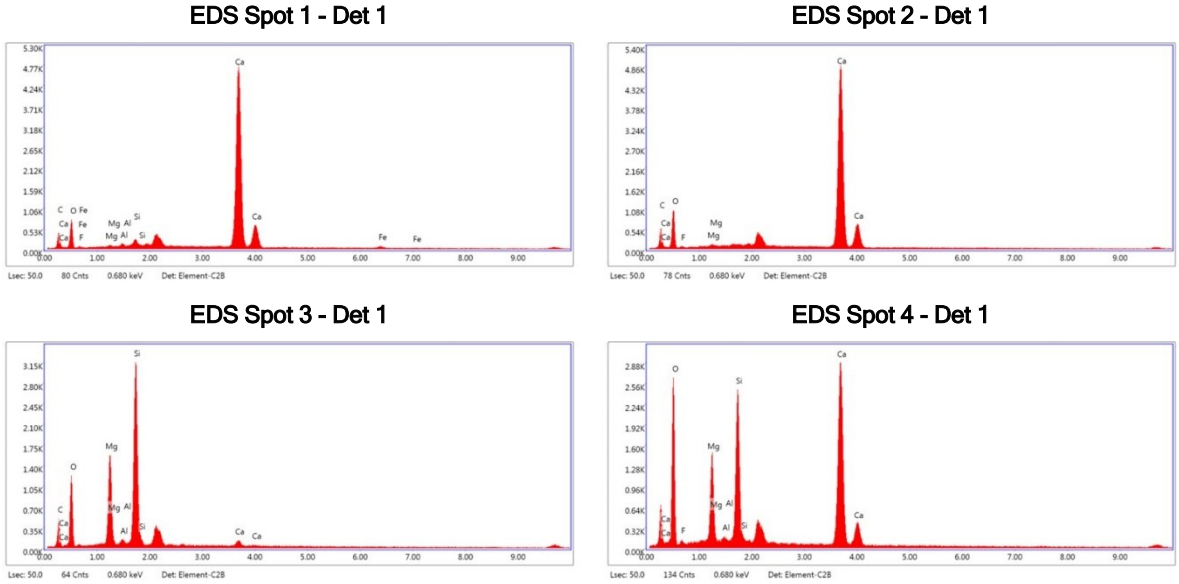

Figure 26 EDS microanalysis of sample CM_69 with areas highlighted in Figure 25

6.2.2. Group 2: CM_89

The binder fraction of CM_89 presents high percentages of Ca, Mg, Al and Si. This can be attributed to the presence of a mixed interplay of C-A-S-H and M-A-S-H phases in the binder matrix. This is consistent with the observations made based on the optical microscopy, indicating some extent of both carbonation of lime and pozzolanic reactions being caused by the ceramic fragments. (Figure 27 and 28)

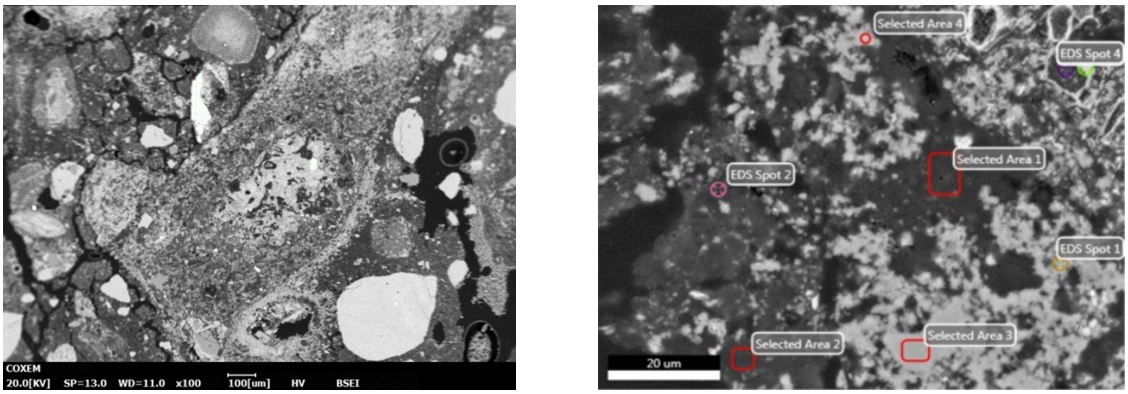

Figure 27 SEM-BSE micrographs of the sample showing a lump at 100x magnification (left) and focused on the lump at 2.0kx highlighting selected areas of EDS analysis (right)

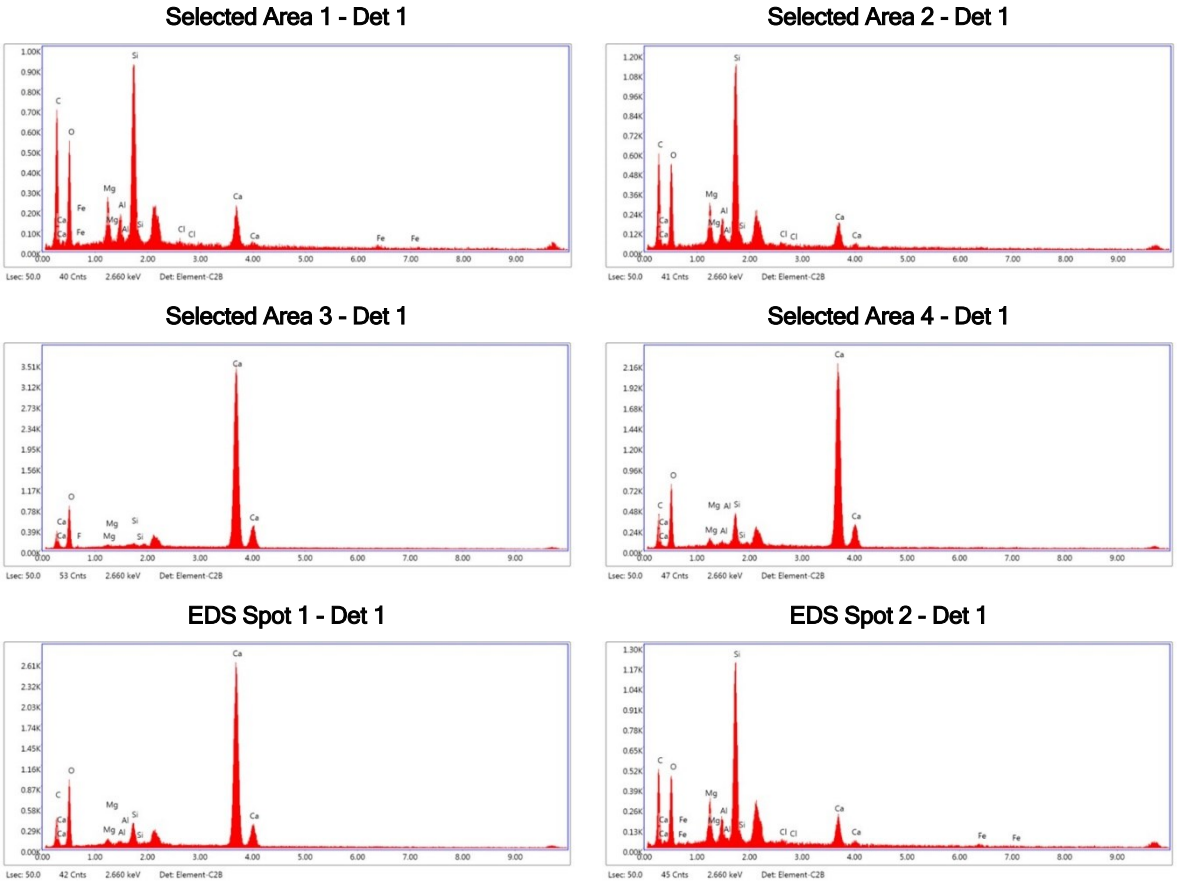

Figure 28 EDS microanalysis of sample CM_89 with areas highlighted in Figure 27

The aggregate fraction shows variations in the intensity of peaks of Ca and Si, with minor peaks of Mg and Al. This is in accordance with the observations made with the optical microscopy showing spots with major percentage of calcium representing limestone aggregates, while spots with major percentage of silicon indicating the ceramic fragment. (Figure 29 and 30)

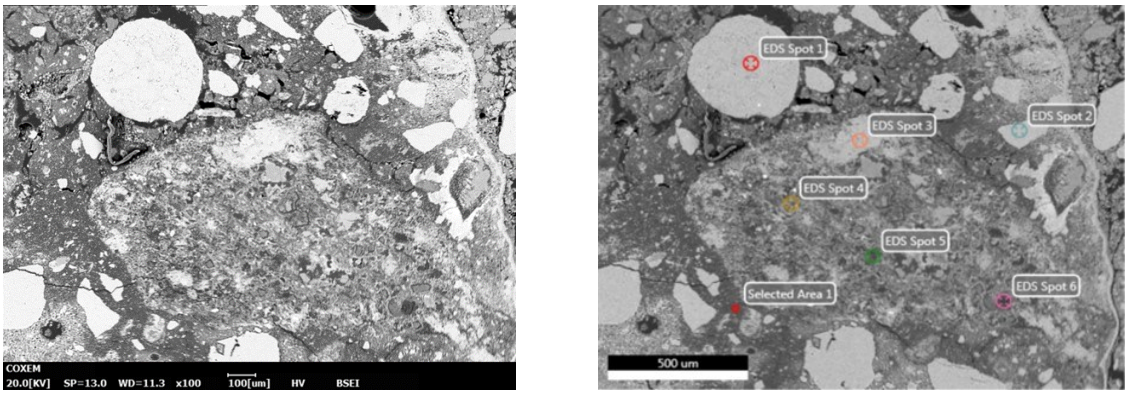

Figure 29 SEM-BSE micrographs of the sample showing aggregates at 100x magnification (left) and highlighting selected areas of EDS analysis (right)

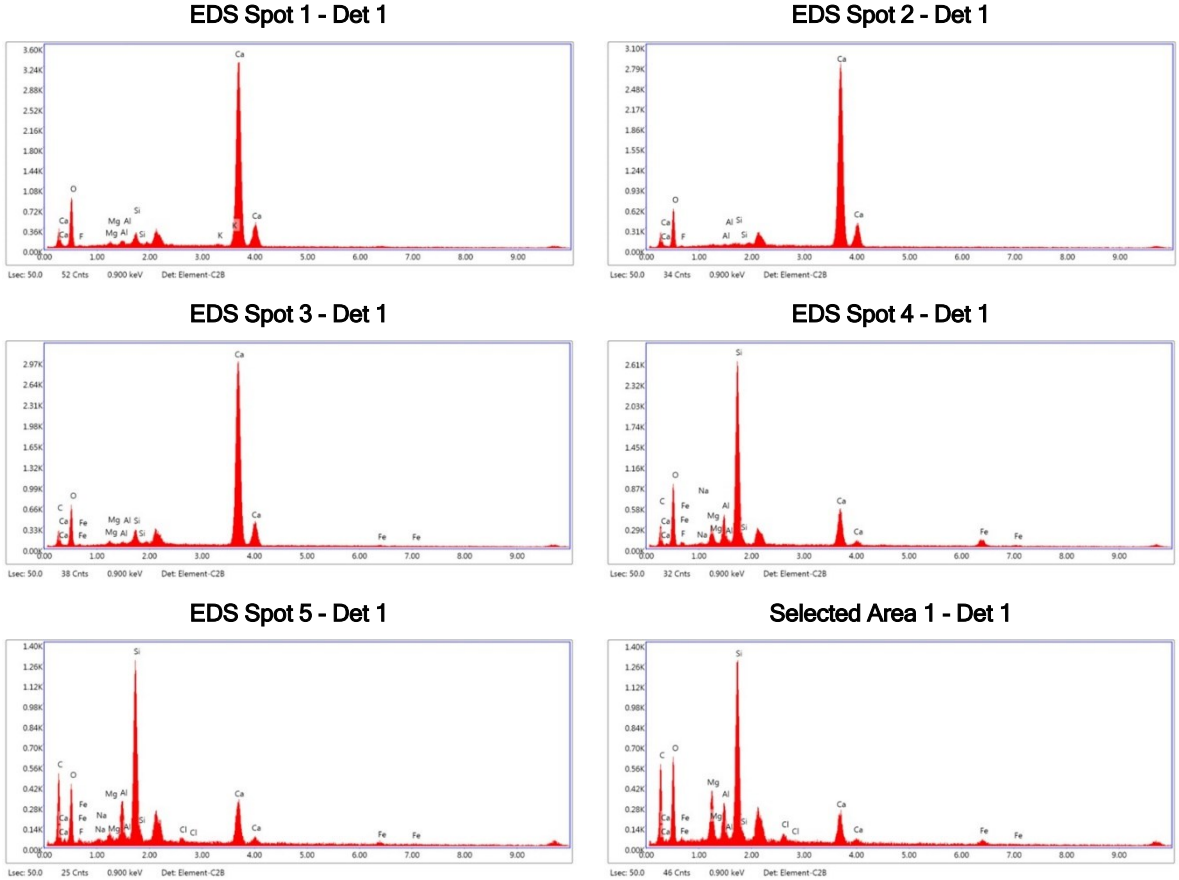

Figure 30 EDS microanalysis of sample CM_89 with areas highlighted in Figure 29

6.2.3. Group 3: CM_66

The binder fraction of CM_66 presents high percentages of Si across all the points, while majority of the selected areas and points also show noticeable peaks of Ca. This is an indicator of a lime-based binder having been modified by the addition of the ceramic fragments and ceramic dust, promoting pozzolanic reactions, resulting in the formation of M-(A)-S-H phases by side of macrozones completely carbonated. This is inferred by the EDS data showing the interaction of calcium with the siliceous and aluminosilicate components of ceramics. (Figure 31 and 32)

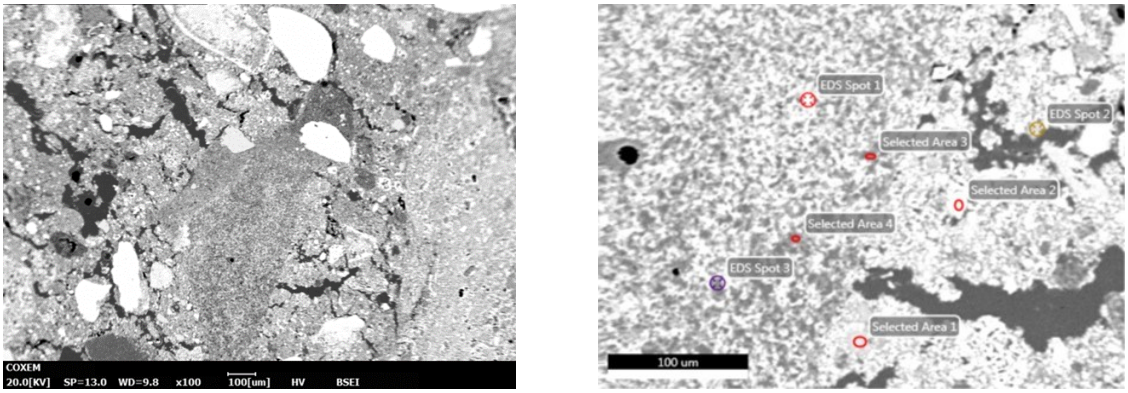

Figure 31 SEM-BSE micrographs of the sample showing a lump at 100x magnification (left) and focused on the lump at 500x highlighting selected areas of EDS analysis (right)

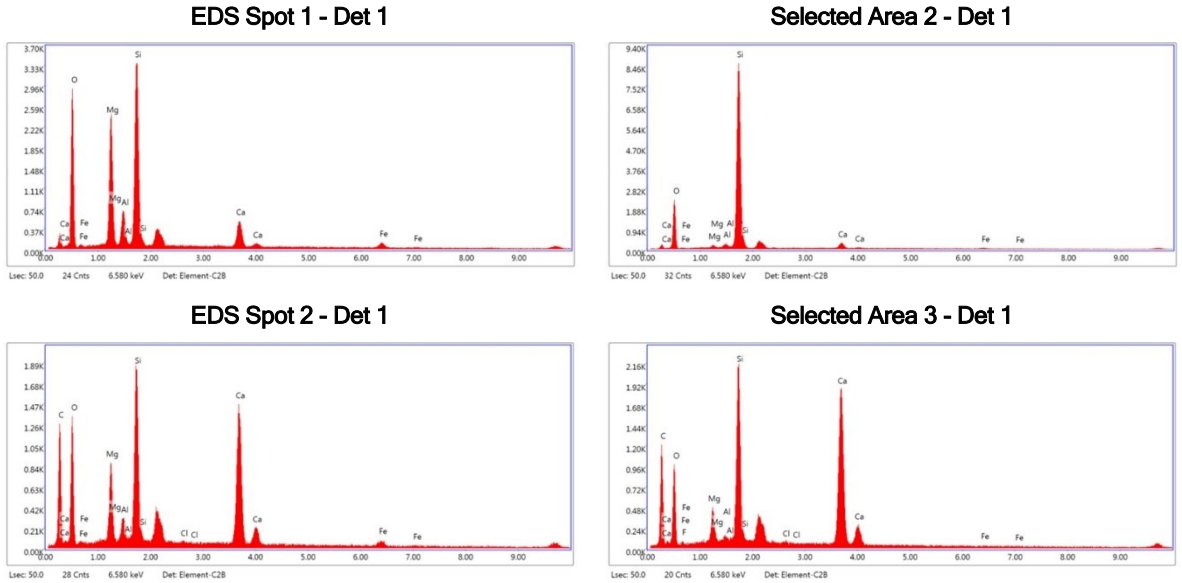

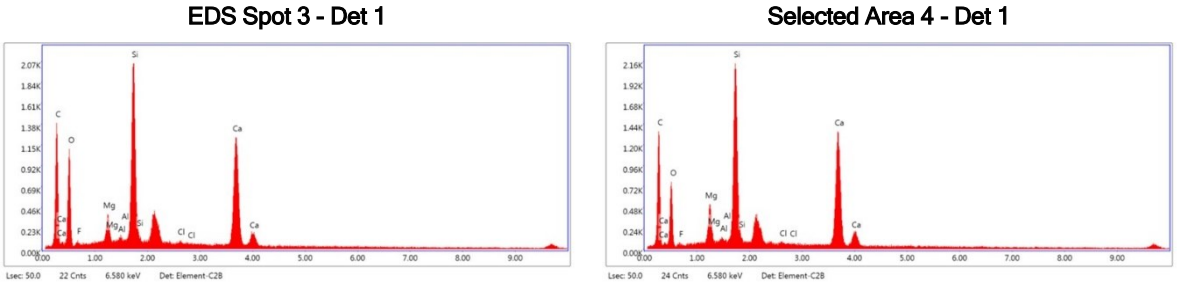

Figure 32 EDS microanalysis of sample CM_66 with areas highlighted in Figure 31

The aggregate fraction confirms the presence of ceramic fragments and ceramic dust in the mortar mix by the recurring peaks of Si, Al, Fe and Ca. This suggests presence of ceramic inclusions undergoing pozzolanic reactions with the lime, contributing to the formation of C-A-S-H/AFm phases in the binder fraction. Overall, the sample is a composite material with calcareous components actively interacting with siliceous and aluminosilicate components.

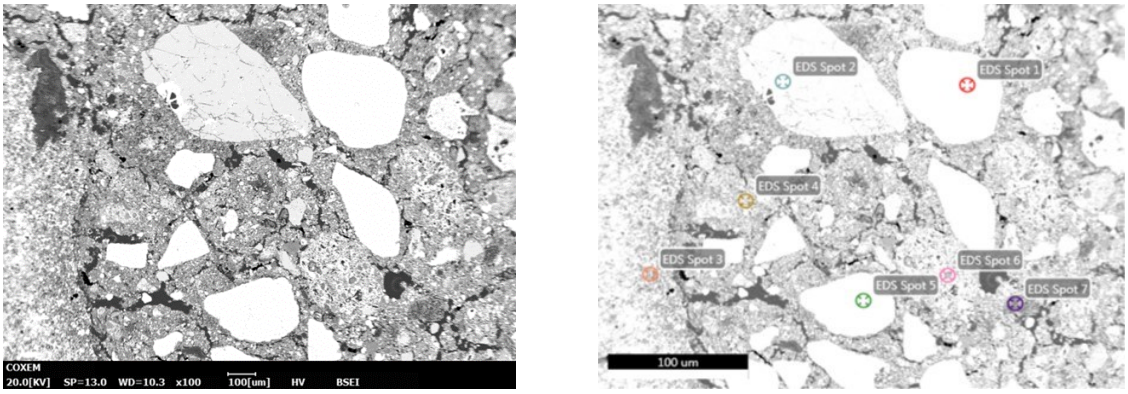

Figure 33 SEM-BSE micrographs of the sample showing aggregates at 100x magnification (left) and highlighting selected areas of EDS analysis (right)

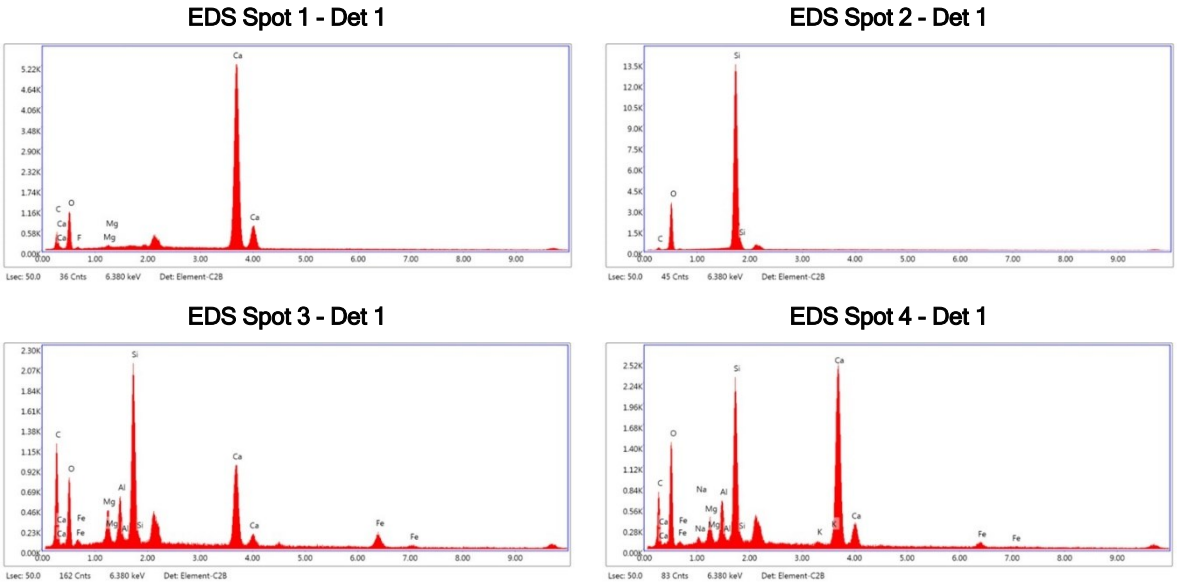

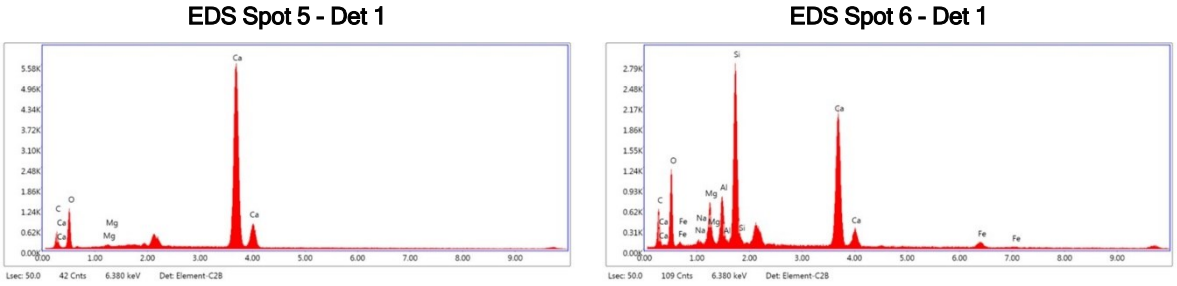

Figure 34 EDS microanalysis of sample CM_66 with areas highlighted in Figure 34

6.2.4. Outlier: CM_76

The binder fraction of CM_76 presents high percentages of Si, and moderate percentages of Ca and Mg, which can be attributed to the formation of M-S-H phases. Despite the absence of sand, as observed by optical microscopy, the mortar has developed a siliceous character, likely due to reaction the cherty limestone/dolostone fragments used in the mix. (Figure 35 and 36)

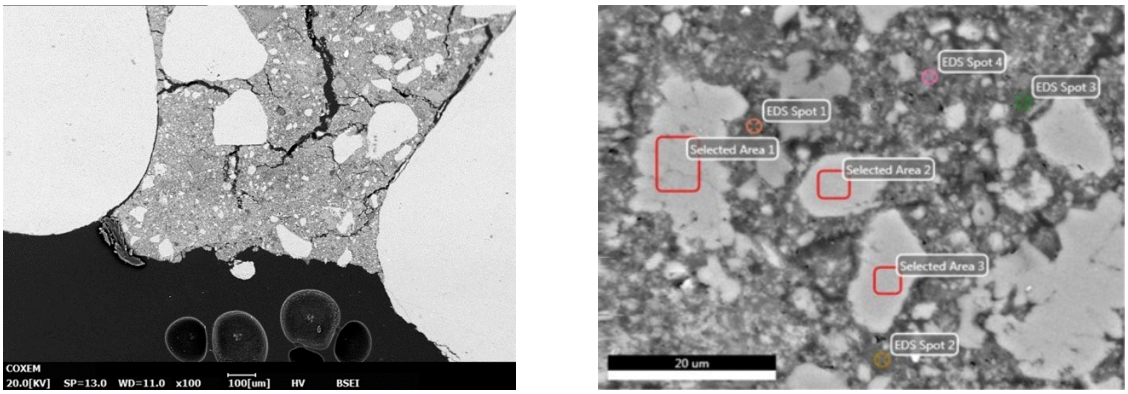

Figure 35 SEM-BSE micrographs of the sample showing binder and aggregates at 100x magnification (left) and highlighting selected areas of EDS analysis (right)

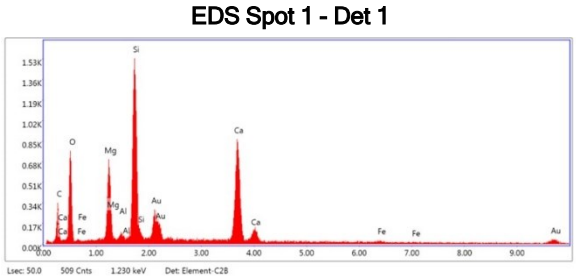

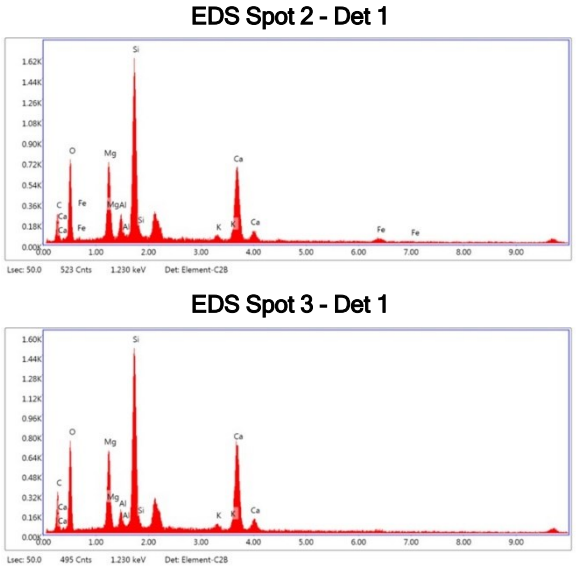

Figure 36 EDS microanalysis of binder fraction of sample CM_76 with areas highlighted in Figure 35

However, most of the aggregate fraction of the sample shows intense peaks of Ca, indicating these to be primarily limestone fragments, as observed by optical microscopy.

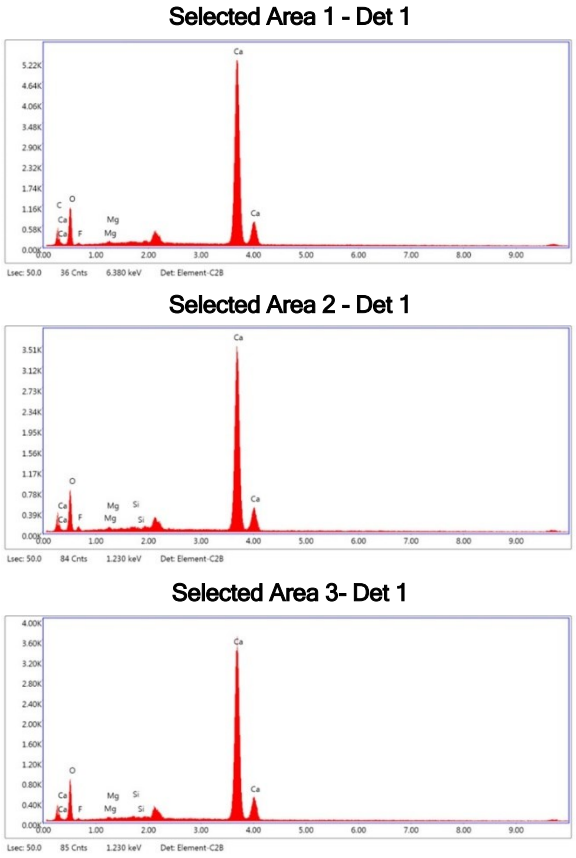

Figure 37 EDS microanalysis of aggregate fraction of sample CM_76 with areas highlighted in Figure 35

6.2.5. Diocletian baths: DB_V1

The binder fraction of DB_V1 presents high percentages of Ca, which is in accordance with the observations from optical microscopy defining it as microsparitic lime-based binder.

The pozzolans in the sample contain both Si and Al, which is consistent with the geological materials from the Alban hills. The overall binder presents lime-based pozzolanic mortar characteristics, where the pozzolans enhance the binder's properties through pozzolanic reactions. (Figures 38 and 39)

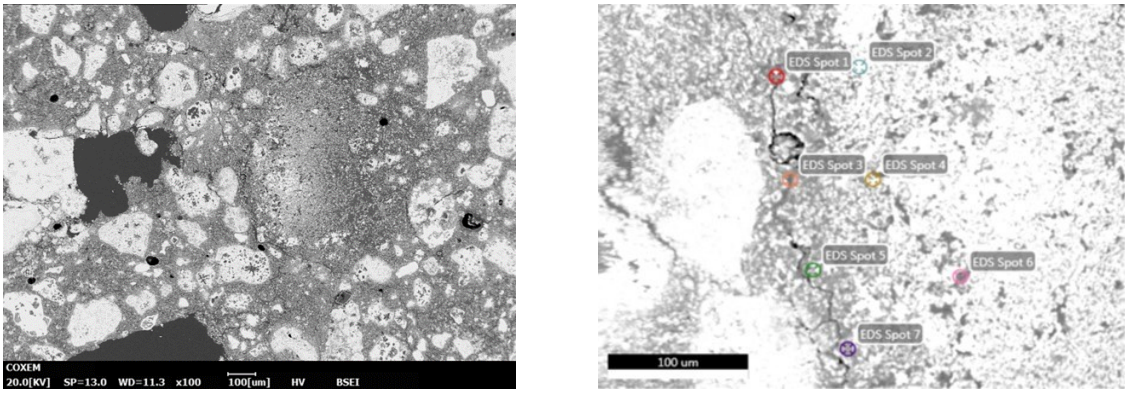

Figure 38 SEM-BSE micrographs of the sample showing a lump at 100x magnification (left) and focused on the lump at 500x highlighting selected areas of EDS analysis (right)

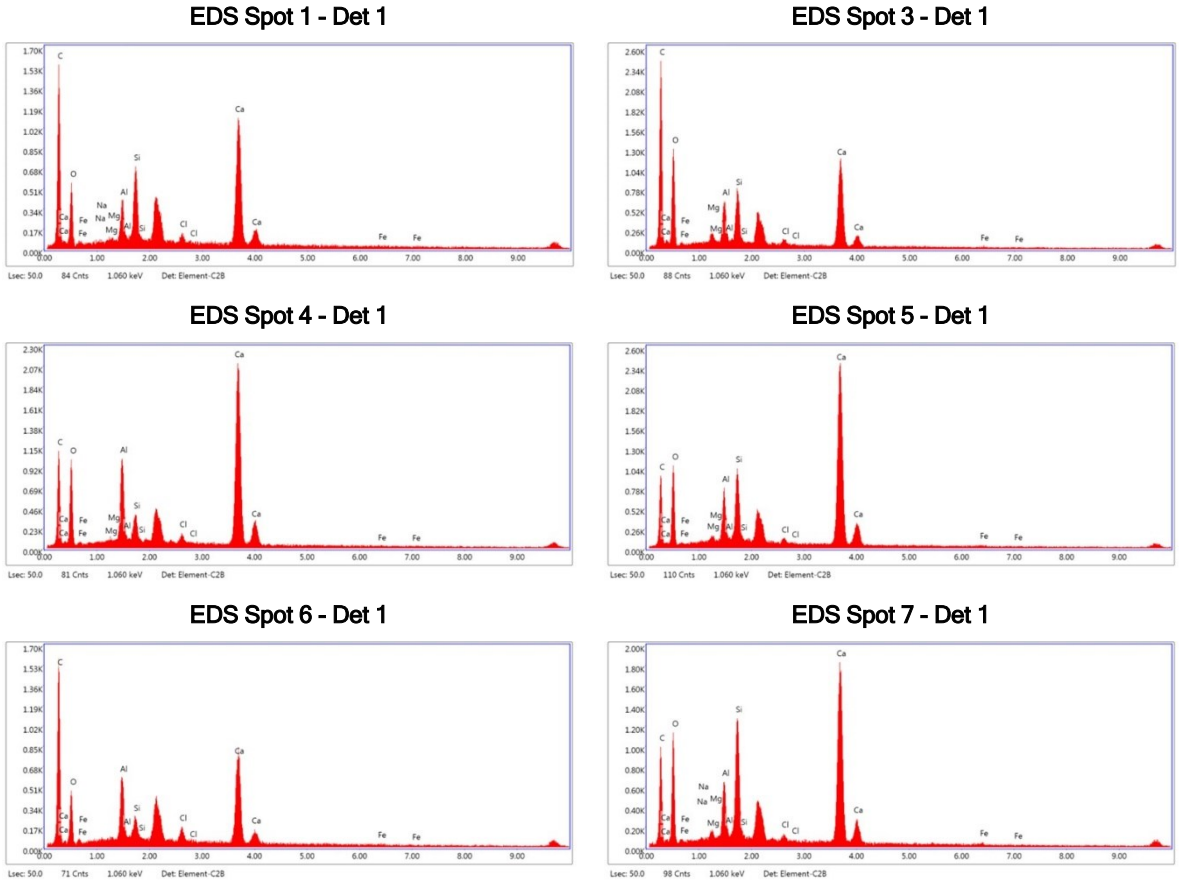

Figure 39 EDS microanalysis of sample DB_V1 with areas highlighted in Figure 38

The aggregate fraction of the sample shows variations between the intensity of peaks of Si, Ca and Al, with a secondary presence of Mg, Fe and Cl. This suggests that the aggregates are a aluminosilicate-rich pozzolanas and tuffs from the Alban Hills. The varying quantities of Mg,

Cl, Fe and Mn indicate that the aggregates exhibit varying minor components and potential impurities. (Figures 40 and 41)

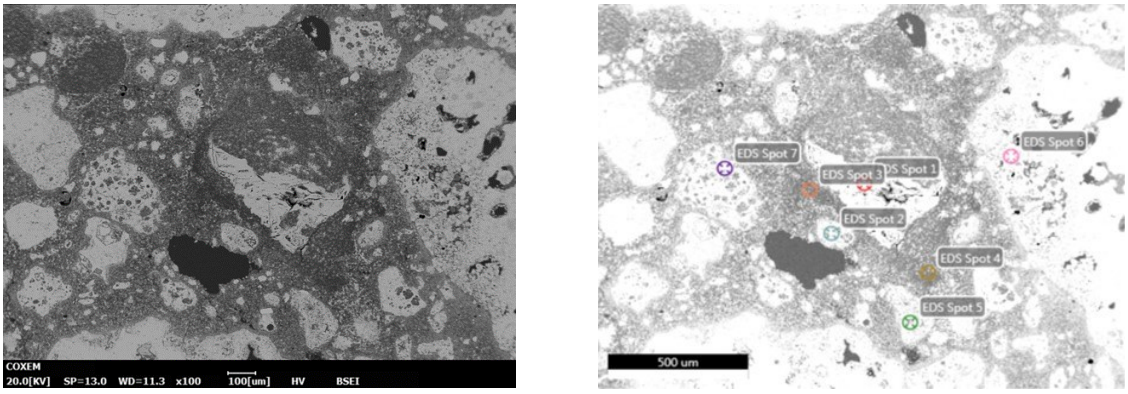

Figure 40 SEM-BSE micrographs of the sample showing aggregates at 100x magnification (left) and highlighting selected areas of EDS analysis (right)

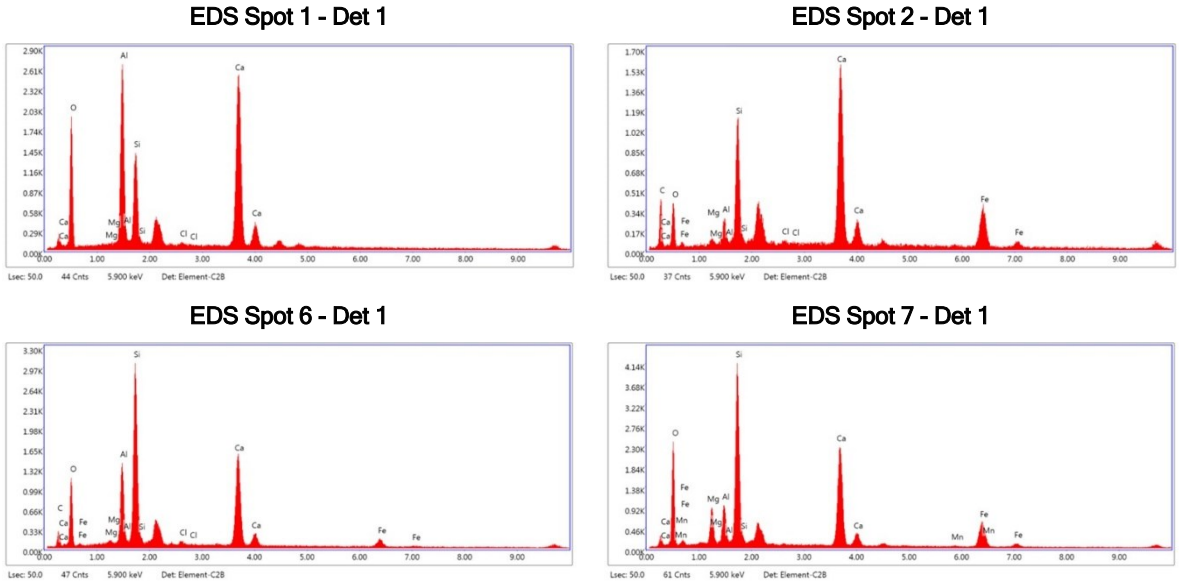

Figure 41 EDS microanalysis of sample DB_V1 with areas highlighted in Figure 40

6.3.XRPD

All 16 samples were analyzed to facilitate a quantitative comparison to the mortar aggregates. The mineral constituents were identified and quantified as weight percentages of the total sample, using High Score Plus for qualitative analysis and Bruker's Topas Diffrac PLUS for quantitative phase analysis.

6.3.1. Aquileia

The results from this analysis confirm the general classes of mortars defined by optical microscopy.

Calcite is the predominant carbonate phase in all samples. This indicates the presence of carbonation products of $Ca(OH)_2$, but it is also a consequence of the calcite in the limestone. Aragonite is a metastable carbonate product only present in the samples with *coccio-pesto* (Group 2 and 3), as a result of the pozzolanic reaction occurring instead of calcination of the binder. (Barnes and Benson 2002) Dolomite, a further carbonate component, is present due to the use of dolomitic limestone in the aggregates.

Hydrocalumite, a C-A-H product (also referred to as AFm phase) also represents a mineral type only present in the *coccio-pesto* mortars (Group 2 and 3), as it is also a result of pozzolanic reaction. This is considered a direct indicator of some level of hydraulicity in the mortar.

Quartz, albite, microcline, muscovite and clinochlore are present in all samples and are indicators of the sand fraction of the mortar. Ilmenite also represents the sand fraction sourced from riverbeds and used as a temper in ceramics.

Some other mineral phases that are only found in the *coccio-pesto* mortars (Group 2 and 3) include hematite, diopside and gehlenite; typical high temperature ceramic phases, tobermorite, a common C-S-H phase from the pozzolanic reaction, and analcime; a crystallization product of the glass present in the ceramics.

Overall, the samples with *coccio-pesto* (Group 2 and 3) exhibit a bigger percentage of amorphous phases compared to Group 1 and the outlier sample.

Table 9 represents the percentage compositions of all the mortar samples from Aquileia.

Table 9 Mineralogical composition of Aquileia mortar samples from XRPD analysis

Group	Sample	Calcite	Aragonite	Hydrocalumite	Dolomite	Quartz	Albite	Microcline	Muscovite	Clinochlore	Hematite	Ilmenite	Diopside	Gehlenite	Tobermorite 14A	Analcime	Amorphous
Group 1: Lime mortar (Sand/Sand with gravel)	**CM_69**	56.87	0.00	0.60	0.66	6.33	0.99	0.18	0.97	1.22	0.00	0.26	0.00	0.00	0.00	0.00	11.91
	CM_88	53.20	0.00	0.00	6.58	9.09	1.17	0.42	0.48	1.19	0.00	0.31	0.00	0.00	0.00	0.00	7.56
	CM_91	56.96	0.00	0.00	1.85	9.23	0.92	0.27	0.76	1.03	0.00	0.34	0.00	0.00	0.00	0.00	8.64
	CM_74	73.95	0.00	0.00	2.88	2.66	0.41	0.21	0.38	0.00	0.00	0.00	0.00	0.00	0.00	0.00	0.00
Group 2: *Coccio-Pesto* with ceramic fragments, no ceramic dust	**CM_70**	64.89	0.00	0.48	0.28	5.13	0.71	0.37	0.51	1.18	0.00	0.21	0.00	0.00	0.00	0.00	6.24
	CM_85	44.64	0.00	1.72	2.82	5.60	1.34	1.88	0.74	1.15	0.32	0.13	5.95	1.45	0.00	0.70	11.56
	CM_89	51.90	4.13	2.66	0.68	4.53	0.76	0.37	0.75	1.29	0.00	0.21	2.56	0.40	0.00	0.00	9.75
Group 3: *Coccio-Pesto* with a ceramic dust	**CM_65**	27.55	0.37	1.21	0.00	8.73	1.18	1.64	2.94	0.75	0.28	0.31	6.35	4.15	0.00	0.00	24.55
	CM_66	37.94	0.91	1.08	0.34	5.90	1.16	1.30	0.41	0.65	0.23	0.05	10.18	2.95	1.26	0.00	15.63
Outlier	**CM_76**	75.38	0.00	0.00	0.54	2.53	0.69	0.42	0.00	0.00	0.00	0.34	0.00	0.00	0.00	0.00	0.09

6.3.2. Diocletian Baths:

In the samples from Diocletian baths, the predominant carbonate phases are represented by calcite and vaterite. The presence of the metastable polymorph vaterite in these samples is an indicator of pozzolanic reaction. These samples contain stratlingite, which is a typical C-A-S-H phase from pozzolanic reaction. This is due to the use of Roman pozzolans which are marked by a high alumina content. Leucite, a feldspathoid (potassium aluminosilicate), is also present in the samples, and it is typical of high potassium and alumina pozzolans of the Colli Albani.

Biotite in the samples is present as it's a common accessory mineral of the pyroclastic materials which are present in the form of tuffs in the samples. Forsterite, a magnesium-rich olivine, is also typical in pozzolanic materials. Analcime is formed as a result of the mineralization of the amorphous glass of pyroclastic products. Hematite and magnetite are the iron oxides present in the samples due to the pozzolans. Hematite could be ascribed to the Pozzolane Rosse fraction, while magnetite to the Pozzolane Nere, both making up the biggest fraction of the aggregates in the samples from Diocletian Baths.

Overall, the amorphous content of these samples is also considerably higher due to the pozzolanic nature of the mortar.

Table 10 represents the percentage compositions of all the mortar samples from the Diocletian baths.

Table 10 Mineralogical composition of Diocletian baths mortar samples from XRPD analysis

Sample	Calcite	Vaterite	Stratlingite	Diopside Ferrain	Leucite	Biotite Ti-rich	Forsterite ferroan	Analcime	Hematite	Magnetite	Amorphous
DB_C1	5.07	2.97	0.40	20.87	8.25	0.97	0.33	7.17	1.06	1.12	31.78
DB_C2	8.58	0.49	0.00	17.52	8.11	0.86	0.08	7.12	1.14	1.16	34.93
DB_C3	6.10	4.09	0.56	18.45	5.99	0.00	0.00	5.98	0.98	1.11	36.75
DB_C4	4.56	2.91	0.31	18.50	8.90	0.82	0.41	5.75	0.47	1.58	35.78
DB_V1	6.55	2.08	1.04	17.80	0.00	0.00	0.00	3.61	1.07	0.85	37.55

6.4. Mechanical Testing

For the tests carried out on the Aquileia samples (CM70 and CM74), a 10-tons cell (Figure 42) and the machine available at the Geosciences Rock Mechanics laboratories (CONTROLS) were used. For the smaller cores from the Baths of Diocletian (V1A.c, V1B.c, V2.c - compression - V1.s and V2.s - splitting), the 2.5 tons cell was used instead. (Figure 43)

(a) (b) (c)

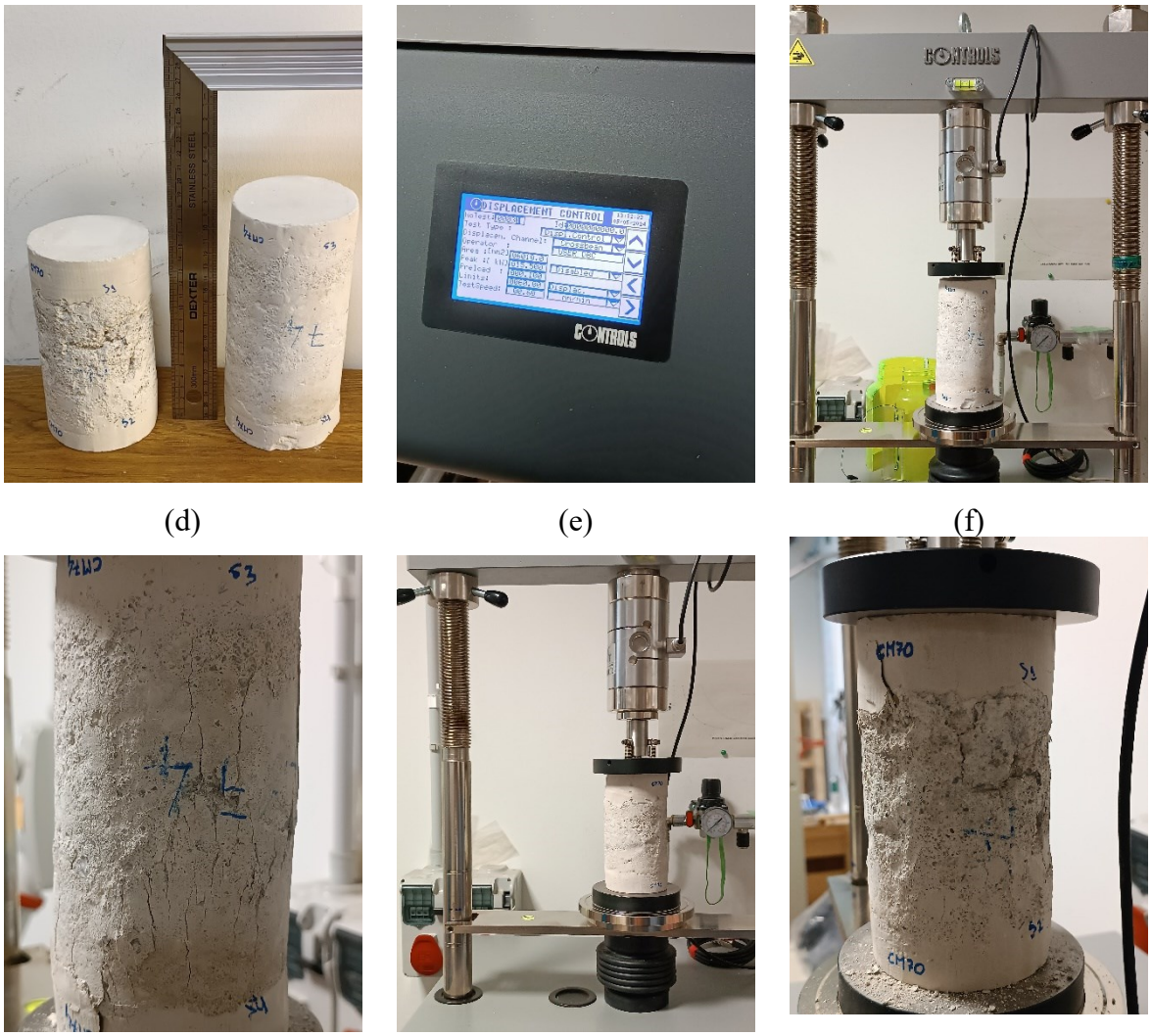

(d) (e) (f)

Figure 42 (a) Samples CM_70 and CM_74 (b) CONTROLS machine interface (c) CM_74 under 10 ton cell in compression (d) Compression failure of the CM_74 sample (e) CM_70 under 10 ton cell in compression (f) Compression failure of the CM_70 sample

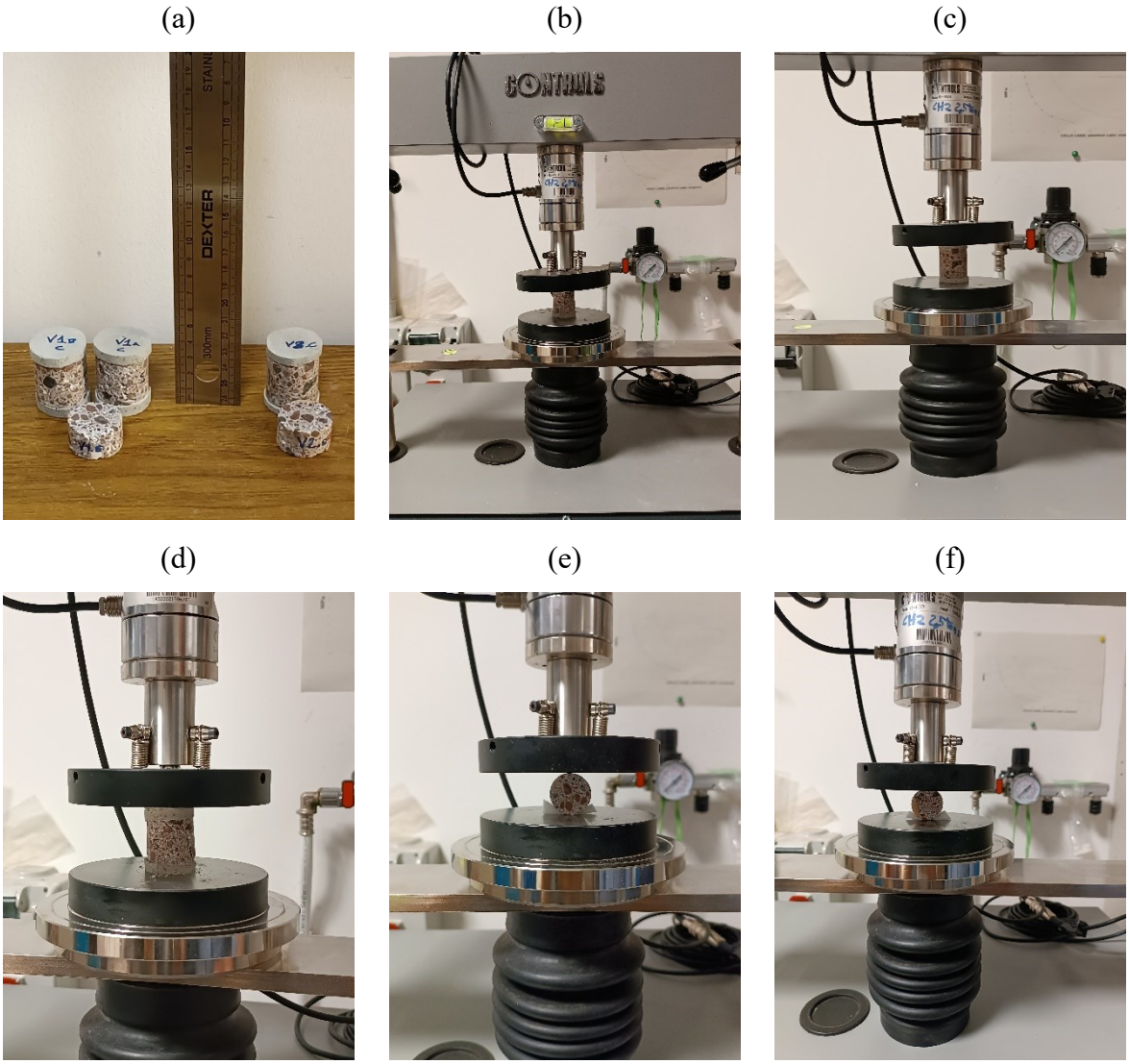

Figure 43 (a) Samples DB_v1 a & b and DB_V2 (b) DB_V1 under 2.5 ton cell in compression (c) Compression failure of the DB_V1a sample (d) Compression failure of the DB_V1b sample (e) DB_V1 under 2.5 ton cell in splitting (f) DB_V2 under 2.5 ton cell in splitting

Due to the irregular and non-standardized dimensions of the samples, a correction factor (formula 3) was applied to the samples with slenderness higher than 1.5, (Panizza et al., 2020) due to the 'tendencies for an increase in the compressive strength of cement mortars as the ratio of small size to standard size samples results about the slenderness and length of the sample base edge' (Drdácký et al., 2013).

$$\frac{f_{c,ref}}{f_c} = \frac{0.983}{0.8766 + 0.26466\,.\ (\phi/h)} \qquad (3)$$

A preliminary observation based on the force-displacement graphs of the compressive strength testing is that the results on the samples from Diocletian baths exhibit higher strength than the ones from Aquileia. This can be attributed to several factors. As evidenced by the XRPD and microscopy results, the Diocletian Baths concretes employed mainly pozzolanic

aggregates which in turn promote the pozzolanic reactions in the binder more than the carbonation reactions, enhancing the strength of the binder significantly compared to the samples from Aquileia. Moreover, the Diocletian Baths mortars also employ smaller aggregates as evidenced by the optical microscopy, which facilitates the transfer of load over a greater surface area and reduces the stress in the mortar. (Figure 44)

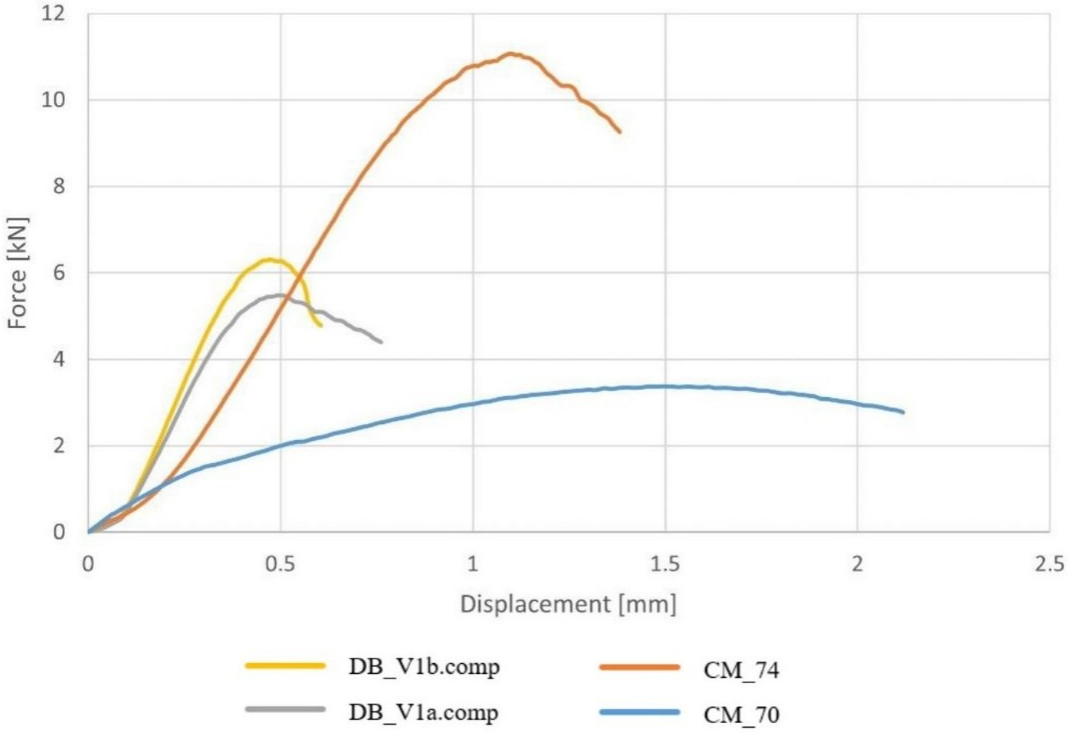

Figure 44 Compressive Strength Test Results in terms of load (N) and displacement (mm)

Another observation that can be made by comparing the results of the samples exhibiting the highest strength is the presence of higher amorphous content, pozzolanic reaction products in the form of vaterite and C-A-S-H phases in the form of stratlingite. These indicate a strong hydraulic character which provides greater adhesion between the binder and the aggregates. This, in conjunction with the use of smaller aggregates and increased surface area of adhesion can be a potential reason behind the exceptional strength of these samples.

Additionally, the presence of imperfections in the samples can cause failure during the tests. In the case of sample DB_V2, a small portion of brick from the masonry was incorporated in the core. This can also be considered as a potential reason for the slight difference in the compressive strength from DB_V1.

Both samples from the Diocletian Baths were also subjected to a splitting test to measure their tensile strength. The results show that the tensile strength of our samples is about 8-9%

of the compressive strength, which is within a normal range for concrete. This ratio is expected, as concrete is typically much weaker in tension than in compression due to its brittle nature. (Figure 45)

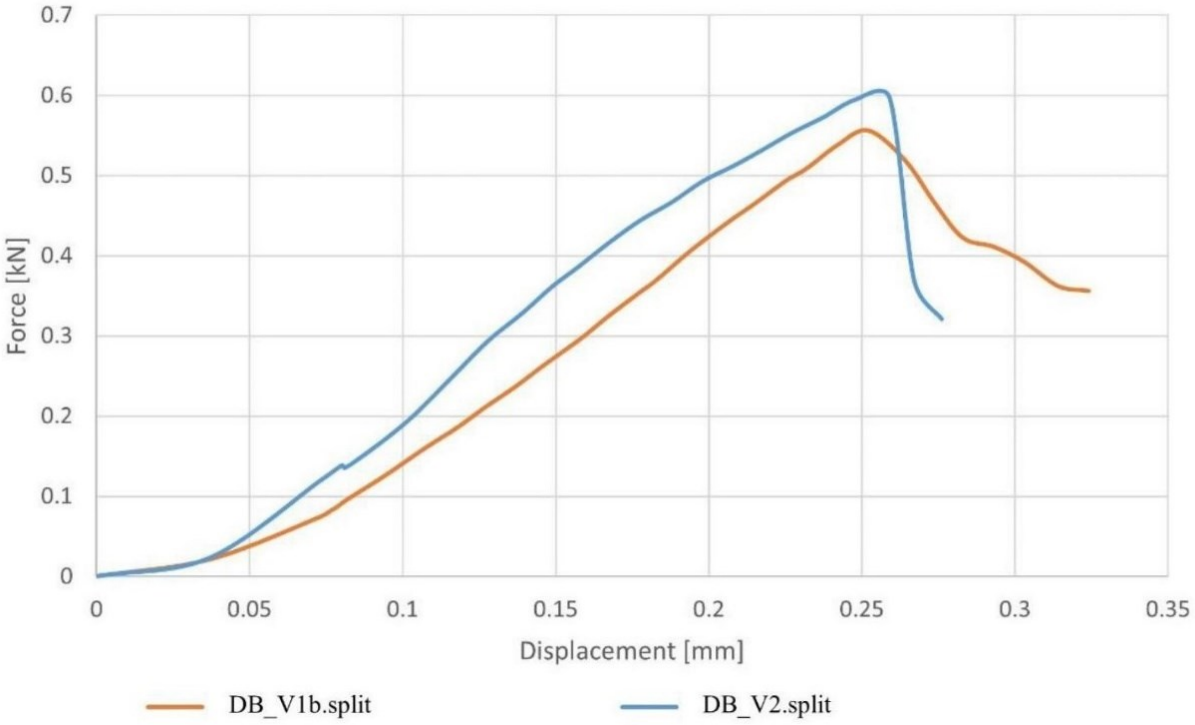

Figure 45 Splitting Strength Test Results in terms of load (N) and displacement (mm)

Table 11 presents the measured ultimate load, compressive strength, and corrected compressive strength for each sample. The observed variation in results can be attributed to the differing textural and granular characteristics of the limestone aggregates. All the samples underwent compression testing, however due to the fragmentary nature of the samples from Aquileia, they were not subjected to the splitting test.

Table 11 Results of the compression and splitting tests

Sample	ϕ (mm)		h (mm)		h / ϕ ratio	Normalising factor	Weight (g)	Cross-section area (mm^2)	Splitting area (mm^2)	Apparent density (g/cm^3)	Compressive strength (Mpa)	Normalised Compressive strength (Mpa)	Splitting strength (Mpa)
CM70	84.20	84.67	158	157.33	1.86	0.973	1520	5630.08		1.716	0.60	0.62	
	85.50		157										
	84.30		157										
CM74	87.00	87.50	185	186.67	2.13	0.991	2520	6013.20		2.245	1.84	1.86	
	88.50		188										
	87.00		187										
V1a.comp	27.70	27.73	39	39.00	1.41	1.015	41.93	604.08		1.780	9.07	8.94	
	27.80												
	27.70												
V1b.comp	27.80	27.80	39.7	39.70	1.43	1.014	43.79	606.99		1.817	10.39	10.24	
	27.80												
	27.80												
V2. comp	27.80	27.73	38.4	38.40	1.38	1.016	40.31	604.08		1.738	9.85	9.69	
	27.70												
	27.70												
V1. split	27.80	27.80	16.1	16.10			15.14	606.99	447.58	1.549			0.849
	27.80												
	27.80												
V2. split	27.60	27.60	16.3	16.30			15.05	598.28	449.88	1.543			0.787
	27.60												
	27.60												

7. Discussion and Conclusions

The theater of Aquileia and the Diocletian Baths, constructed in early imperial age (beginning of the 1st century AD) and in the late imperial age in the 4th century AD respectively, present a complex case study of historical construction techniques and materials. With this research project, we conducted an archaeometric analysis of the structures to identify and compare the chemical, mineralogical and mechanical characteristics of the structural mortars.

The characterization was performed through the application of four diverse analytical methods: Optical microscopy, Scanning electron microscopy with energy-dispersive X-ray spectroscopy (SEM-EDS), X-ray powder diffraction (XRPD), and Compressive and splitting strength tests. This comprehensive approach allowed us to examine the materials at various levels of analysis.

The first stage of analysis helped us with confirming the frequent use of lime with different pozzolanic additions across all mortars and categorizing the mortars based on the type of aggregate used. This was supported by the attribution of the Aquileia samples into four distinct groups, while the samples from Diocletian baths showed uniform properties. The use of pozzolanic binder was confirmed by the presence of significant amounts of aggregates facilitating pozzolanic reactions with lime to form various hydrated phases, including C-S-H, C-A-S-H and M-S-H. Furthermore, the occurrence of alkali-carbonate and alkali-silicate reactions, due to the dedolomitization of dolomite aggregates, caused a heightened degree of hydraulicity in the samples with dolomitic and ceramic aggregates, favoring the formation of M-A-S-H phases by side of traditional pozzolanic reaction. This further hydraulic character suggests that the mortars exhibit substantial strength when a pozzolanic aggregate is added to it. However, some samples displayed heterogeneity in the mortar composition, indicating potential inconsistencies in the mixing and production processes, leading the research to the next level of analysis.

The geomaterials available in the two regions where the samples were obtained show distinct characteristics. Notably, in the Roman territory, the local availability of *harenae fossiciae* (fossil sand) from the Alban Hills facilitated the development of more robust and durable structural mortars (see infra mechanical properties). In contrast, the mortars from Aquileia, which are characterized by non-pozzolanic carbonate or siliceous gravels, did not achieve the same pozzolanic properties. As a result, hydraulic mortars in Aquileia were mainly produced by incorporating *coccio-pesto*-based mixtures.

Moreover, earlier mortars from Aquileia were characterized by the aggregates belonging to bigger-sized classes, in contrast to the Diocletian Baths that led us to form the conclusion that usage of smaller aggregates to ensure larger area of reaction surface provides better adhesion between the binder and aggregates. This influenced positively the development of C-S-H and C-A-S-H phases in the mortars from Diocletian baths, that was primarily promoted by the use of local volcanic pozzolans.

On the other hand, the presence of significant pieces of ceramic fragments and powder and indications of mortar reuse in Aquileia also suggest that Romans were aware of the potentiality of pozzolanic reaction of ceramic materials by side of volcanic ones that were not locally sourceable in Friuli. This layers were probably used in water-proofing of of the lowest portion of the foundational structures of the theatre, as already noted in Dilaria et al. 2023.

Finally, the mortar was subjected to the analysis of mechanical properties. The compressive strengths of the test specimens in the study were found to range between 0.6 and 10.24 megapascals (MPa). The observed variations were attributed to the differing textural and compositional characteristics of the mortars, as described in the preceding levels of research. The samples exhibiting the highest hydraulicity, unimodal aggregate distribution and the least anomalies provide the highest strength. The presence of fatter mortars and highly reactive aggregates in the mixes, as well as the use of smaller aggregates, which are more efficient in distributing load, are also huge contributing factors towards this observation.

With this study, we can form the conclusion that compressive strength of the samples is significantly influenced by hydraulic characteristics and imperfections, rather than density alone. Variations in strength are likely due to anomalies in construction techniques and use of aggregates with different reactive properties. For instance, the higher strength of sample DB_V1 may reflect Roman experiments in construction techniques aimed at fortifying the load bearing structures in environments with high moisture by the use of more reactive aggregates.

The characterization of the binders and the analysis of the mechanical properties of mortars is an essential tool for identifying suitable methods and recipes of concrete for restoration purposes, while ensuring the compatibility and sustainability of these methods. Moreover, we also gained important insight into the technological advancements and material choices of the ancient civilizations. Overall, the findings of this study contribute to our broadened knowledge of historical construction practices and provides a solid foundation for future conservation and restoration of these monuments and similar sites.

8. Bibliography

- Ackerman, J.S. (1964) *The Architecture of Michelangelo*. 2nd edn. Viking Press.
- Barnes, P. and Bensted, J. (2002) *Structure and Performance of Cements*. 2nd edn. CRC Press.
- Bartman, E. (2020) 'Rediscovering the rediscovery of antiquity in the Renaissance - BARBARA FURLOTTI, ANTIQUITIES IN MOTION: FROM EXCAVATION SITES TO RENAISSANCE COLLECTIONS', *Journal of Roman Archaeology*, 33, pp. 962-965. doi: 10.1017/S1047759420000811.
- Dilaria, S. and Salvadori, M. (2021) 'Aquileia, quartieri settentrionali: nuovi dati per la ricostruzione dell'organizzazione urbanistica e dell'assetto interno dell'insula delle bestie ferite', *Archeologia Classica*, 72, p. 11. doi: 10.48255/J.ArchCl.LXXII.2021.11.
- Dilaria, S. and Secco, M. (2018) *Anfiteatro di Aquileia: Analisi archeometriche sulle miscele leganti (malte e calcestruzzi)*.
- Dilaria, S., Secco, M., Bonetto, J., Ricci, G., and Artioli, G. (2023) 'Making Ancient Mortars Hydraulic: How to Parametrize Type and Crystallinity of Reaction Products in Different Recipes', in *Advanced Nanomaterials*. doi: 10.1007/978-3-031-31472-8_4.
- Dilaria, S., Secco, M., Ghiotto, A., Furlan, G., Giovanardi, T., Zorzi, F., and Bonetto, J. (2023) 'Early exploitation of Neapolitan pozzolan (pulvis puteolana) in the Roman theatre of Aquileia, Northern Italy', *Scientific Reports*, 13. doi: 10.1038/s41598-023-30692-y.
- Drdácký, M., Fratini, F., Frankeová, D., and Slížková, Z. (2013) 'The Roman mortars used in the construction of the Ponte di Augusto (Narni, Italy) - A comprehensive assessment', *Construction and Building Materials*, 38, pp. 1117–1128. doi: 10.1016/j.conbuildmat.2012.09.044.
- Ghiotto, A.R., Fioratto, G., and Furlan, G. (2021) 'Il Teatro Romano di Aquileia: Lo Scavo Dell'aditus Maximus Settentrionale e Dell'edificio Scenico', *FOLD&R Fasti On Line Documents & Research*, 495.
- Katayama, T. (2010) 'The So-Called Alkali-Carbonate Reaction (ACR) — Its mineralogical and Geochemical Details, with Special Reference to ASR', *Cement and Concrete Research*.
- Leone, G., Vita, A., Consumi, M., Tamasi, G., Bonechi, C., Donati, A., Rossi, C., and Magnani, A. (2019) 'Comparison of Original and Modern Mortars at the Herculaneum

Archaeological Site', *Conservation and Management of Archaeological Sites*, 21, pp. 92-112. doi: 10.1080/13505033.2019.1638139.

- Marra, F., Danti, A., and Gaeta, M. (2015) 'The volcanic aggregate of ancient Roman mortars from the Capitoline Hill: Petrographic criteria for identification of Rome's "pozzolans" and historical implications', *Journal of Volcanology and Geothermal Research*, 308, pp. 113-126. doi: 10.1016/j.jvolgeores.2015.10.007.
- Moropoulou, A., Bakolas, A., and Bisbikou, K. (1995) 'Characterization of ancient, Byzantine and later historic mortars by thermal and X-ray diffraction techniques', *Thermochimica Acta*, 269–270, pp. 779-795. doi: 10.1016/0040-6031(95)02571-5.
- Owsiak, Z. (2024) 'Microscopic methods for analysis of mortars from historical masonry structures', *Bulletin of the Polish Academy of Sciences Technical Sciences*. doi: 10.24425/bpasts.2021.136042.
- Panizza, M., Natali, M., Garbin, E., Ducman, V., and Tamburini, S. (2020) 'Optimization and mechanical-physical characterization of geopolymers with Construction and Demolition Waste (CDW) aggregates for construction products', *Construction and Building Materials*, 264, p. 120158. doi: 10.1016/j.conbuildmat.2020.120158.
- Platner, S.B. and Ashby, T. (1929) *A Topographical Dictionary of Ancient Rome*. 2nd edn. Allyn and Bacon.
- Plevoets, B. and Van Cleempoel, K. (2019) *Adaptive Reuse of the Built Heritage: Concepts and Cases of an Emerging Discipline*. 1st edn. Routledge.
- Rubinich, M., Tiussi, C., Ventura, P., Basso, P., Bonetto, J., Cottica, D., Dilaria, S., Fontana, F., and Ghiotto, A. (2024) 'Aquileia and its urban development in the light of recent and ongoing research'. doi: 10.3986/9789610508281_03.
- Secco, M., Dilaria, S., Bonetto, J., Addis, A., Tamburini, S., Preto, N., Ricci, G., and Artioli, G. (2020) 'Technological transfers in the Mediterranean on the verge of Romanization: Insights from the waterproofing renders of Nora (Sardinia, Italy)', *Journal of Cultural Heritage*, 44, pp. 63-82. doi: 10.1016/j.culher.2020.01.010.
- Secco, M., Maritan, L., Mazzoli, C., Lampronti, G., Zorzi, F., Nodari, L., and Russo, U. (2011) 'Alteration Processes of Pottery in Lagoon-like Environments', *Archaeometry*, 53, pp. 809–829. doi: 10.1111/j.1475-4754.2010.00571.x.
- Secco, M., Valentini, L., and Addis, A. (2019) 'Ancient and Modern Binders: Naturally Nanostructured Materials', in Lazzara, G. and Fakhrullin, R. (eds) *Advanced*

Nanomaterials, Nanotechnologies and Nanomaterials for Diagnostic, Conservation and Restoration of Cultural Heritage. Elsevier, pp. 205-237. doi: 10.1016/B978-0-12-813910-3.00010-0.

- Velosa, A.L., Veiga, R., Coroado, J., Ferreira, V.M., and Rocha, F. (2010) 'Characterization of Ancient Pozzolanic Mortars from Roman Times to the 19th Century: Compatibility Issues of New Mortars with Substrates and Ancient Mortars', in Dan, M.B., Přikryl, R., and Török, Á. (eds) *Materials, Technologies and Practice in Historic Heritage Structures*. Dordrecht: Springer Netherlands, pp. 235–257. doi: 10.1007/978-90-481-2684-2_13.
- Wentworth, C.K. (1922) 'A Scale of Grade and Class Terms for Clastic Sediments', *The Journal of Geology*, 30(5), pp. 377–392. Available at: http://www.jstor.org/stable/30063207 (Accessed: 1 Sept. 2024).